

Experimental calibration of a garnet–clinopyroxene geobarometer for mantle eclogites

C. Beyer · D. J. Frost · N. Miyajima

Received: 10 March 2014 / Accepted: 10 January 2015 / Published online: 6 February 2015
© Springer-Verlag Berlin Heidelberg 2015

Abstract Thermodynamic parameters have been calibrated for a geobarometer suitable for use on eclogitic mantle xenoliths. The barometer is based on the incorporation of tetrahedrally coordinated aluminum in clinopyroxene coexisting with garnet and has been calibrated using the results of piston cylinder and multi-anvil experiments performed between pressures of 3 and 7 GPa and temperatures from 1,200 to 1,550 °C. Starting materials were hydrous and anhydrous synthetic mixtures of basaltic bulk compositions that yielded homogeneous biminerally garnet–clinopyroxene phase assemblages. The experimental data set was expanded by employing results from previous experimental studies conducted in eclogitic systems, which widened the range of applicable conditions and compositions. The calibration reproduces experimental pressures of biminerally eclogite assemblages, in addition to SiO₂-saturated and kyanite-bearing eclogites, to within 0.4 GPa at the 95 % confidence interval. The barometer was then used to examine equilibration pressures recorded by natural mantle eclogites from various xenolith locations covering a wide pressure, temperature, and compositional range.

Keywords Eclogite · Geobarometer · Mantle xenoliths · Cratonic lithosphere

Communicated by Jon Blundy.

Electronic supplementary material The online version of this article (doi:10.1007/s00410-015-1113-z) contains supplementary material, which is available to authorized users.

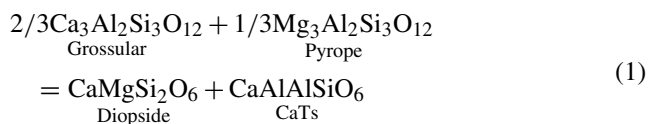
C. Beyer (✉) · D. J. Frost · N. Miyajima
Bayerisches Geoinstitut, University of Bayreuth, 95440 Bayreuth,
Germany
e-mail: christopher.beyer@uni-bayreuth.de

Introduction

Geobarometry measurements are essential for understanding the thickness, thermal structure, and tectonic evolution of the lithosphere in addition to providing vital information on the depth of magmatic and metasomatic processes evident in mantle xenoliths (Rudnick et al. 1998; Griffin et al. 2003; Kopylova et al. 2004). Eclogite rocks are formed from mafic protoliths within high-grade metamorphic belts and ultrahigh-pressure terrains where their presence indicates pressures of at least 1 GPa (Liou et al. 2009). Eclogites are also found as mantle xenoliths in kimberlites erupted within the cratonic lithosphere, whereby the occasional presence of diamonds indicates equilibration pressures of at least 4 GPa, i.e., greater than 120 km depth (Jacob 2004; Schulze 1989). Eclogitic rocks account for only a small percentage of mantle xenoliths from such localities (Schulze 1989), but their significance outweighs their abundance for several reasons. Eclogitic xenoliths are of economic interest due to their higher yield of diamonds relative to peridotitic xenoliths (Cartigny 2005; Stachel and Harris 2008). Due to their proposed origin as mafic oceanic crustal rocks, they would seem to trace subduction processes related to the assembly (Helmstaedt and Doig 1975; Jacob 2004; MacGregor and Manton 1986) and evolution (Griffin et al. 2003; Rapp et al. 1991; Shirey et al. 2001) of the cratonic lithosphere. However, it has also been proposed that at least some eclogite xenoliths are magmatic rocks formed as deep seated cumulates (Smyth et al. 1989; Taylor and Neal 1989). Due to their potentially central role in the formation and evolution of the cratonic lithosphere, it is important to be able to reconstruct the pressure and temperature conditions at which eclogitic xenoliths last equilibrated.

Over the last decades, several efforts have been made to calibrate geobarometers suitable for the determination of the depth at which eclogite rocks have equilibrated (e.g., Ashchepkov et al. 2010; Nimis and Ulmer 1998; Simakov 2008). Most of the experimental calibrations, however, have been limited to a relatively narrow range of pressure, temperature, and bulk composition, and many of the reactions investigated employ accessory phases, such as olivine, cordierite, quartz, kyanite, orthopyroxene, and mica that are not always present in eclogite rocks (Brey and Köhler 1990; Coleman et al. 1965; Newton and Perkins 1982; Nickel and Green 1985; Nikitina 2000; Nimis and Taylor 2000). In order to compare the equilibration conditions of eclogites worldwide, it is important to be able to employ a geobarometer that is based only on garnet and clinopyroxene (cpx) that are present in all eclogites. This has proved difficult, however, (Koons 1984; Mukhopadhyay 1991; Newton 1986), and has been proposed to be also complicated by metasomatic overprinting (Liu et al. 2009; Smart et al. 2009; Tappe et al. 2011). Only a few such studies exist, and these are either limited in their application by the chemical system (e.g., CMAS and Cr content), the narrow compositional range of the calibration, or by the reliance on data from non-eclogitic assemblages (Brey et al. 1986; Mukhopadhyay 1991; Nimis and Taylor 2000; Simakov and Taylor 2000; Simakov 2008). The significant jadeite (Jd) component in eclogitic clinopyroxenes has also been ignored in some studies.

It has long been recognized that Al incorporation in clinopyroxene coexisting with garnet is pressure-dependent (Herzberg 1978; Brey et al. 1986; Mukhopadhyay 1991). In eclogitic clinopyroxene, Al is incorporated through the jadeite ($\text{NaAlSi}_2\text{O}_6$), Ca-Tschermaks ($\text{CaAlAlSi}_2\text{O}_6$), and Ca-Eskola ($\text{Ca}_{0.5}\square_{0.5}\text{AlSi}_2\text{O}_6$) components. While Ca-Eskola is a minor component in the majority of eclogites (Simakov 2008), Ca-Tschermaks is common, with concentrations of up to 25 mol % (Dawson and Carswell 1990) and the jadeite component can range up to 70 mol % in kyanite- or corundum-bearing eclogites (O'Reilly and Griffin 1995). As the proportion of the Ca-Tschermak (CaTs) component had been shown to decrease with pressure (Boyd 1970), Mukhopadhyay (1991) proposed the following equilibrium as a potential geobarometer



This geobarometer was applied successfully to garnet clinopyroxenites (Mukhopadhyay 1991); however, the calibration presented is less suitable for eclogitic clinopyroxenes with high jadeite contents. Simakov (2008) also presented a thermodynamic calibration for this equilibrium

over a wider range of pressure and temperature. However, very little of the data used in this calibration were applicable to natural eclogite compositions, with a significant portion of the employed data being either from very simple systems (Gasparik 1996), peridotitic systems (Walter 1998), or from experiments at more extreme conditions (Ono and Yasuda 1996) than those associated with mantle xenoliths.

Here, we present a new thermodynamic calibration for equilibrium (1), which takes explicit account of the clinopyroxene jadeite component and is based on the results of high-pressure eclogite equilibration experiments. The barometer is, therefore, applicable to natural eclogitic bulk compositions including those that resemble normal mid-ocean ridge basalt (N-MORB). The experimental calibration extends to conditions applicable to eclogite xenoliths from depths of up to 250 km. H_2O was employed as a flux in the experiments to promote equilibrium, and most eclogitic assemblages coexisted with large portions of hydrous silicate melt. The barometer calibration is made more rigorous by the inclusion of additional experimental data sets from previous studies. Finally, the calibration has been applied to several natural suits of eclogitic xenoliths and to some eclogitic diamond inclusions to determine equilibration pressures. The results are also compared with two other geobarometers.

Experimental methods

Rationale

In order to calibrate the compositional evolution of biminerally eclogites as a function of pressure, experiments were conducted in multi-anvil and piston cylinder devices at pressures between 3 and 7 GPa and temperatures of 1,200–1,550 °C. The starting material was a synthetic average “wet” N-MORB composition containing ~2 wt% H_2O . The bulk composition was simplified by the exclusion of minor elements such as K, P, and Cr, but in some experiments, 2 wt% fluorine was also added. In order to ensure chemical equilibrium, experiments were performed in the presence of hydrous melt and initially raised by 50 °C above the final run temperature. This generally ensured complete recrystallization of the solid assemblage, indicated by a lack of chemical zonation. The objective was to obtain chemical equilibrium by performing experiments at temperatures generally higher than those at which many natural eclogitic assemblages equilibrated. These experiments were then used to calibrate parameters in a thermodynamic model that could be reliably extrapolated to lower temperatures. When fitting the thermodynamic model, well-constrained parameters were taken from previous studies (Ganguly

et al. 1996; Holland and Powell 2011). The experimental data were only used to derive non-ideal mixing terms for the clinopyroxene solid solution, for which cation interaction terms on the different sites are poorly constrained, particularly in eclogitic compositions.

Starting material

The principal eclogitic starting material (OC1/2, Table 1), which was an average N-MORB composition (Lehnert et al. 2000), was fabricated from a synthetic mixture of analytical grade oxides and carbonates, which were dried to remove surface water and ground in an agate mortar under acetone. The initial composition was made with a deficit of Al_2O_3 such that it could be added in a final stage as $\text{Al}(\text{OH})_3$ in order to add H_2O to the starting composition. Subsequently, the mix was decarbonated in air by heating it to 1,000 °C for 3 h. The powder was then fused in a Fe-saturated platinum crucible at 1,600 °C in order to obtain a homogenous glass that was reground in an agate mortar under acetone to a fine powder. Iron, originally added to the starting mixture as Fe_2O_3 , was reduced by pressing the powder into a pellet and suspending it in a gas-mixing furnace at 800 °C with a 50:50 $\text{CO}_2\text{--H}_2$ gas mix for 15 h at an f_{O_2} of approximately 2 log units below the fayalite magnetite quartz (FMQ) oxygen buffer. $\text{Al}(\text{OH})_3$, and in some cases CaF_2 , were added to the mixture to provide sources of H_2O and fluorine. 1 wt% of IrO_2 was added to the mixture and acted as a redox sensor (Woodland and O'Neill 1997). After additional grinding to homogenize the mixture, it was dried and denitrified in a drying oven at 140 °C. A series of five more anhydrous bulk compositions (Omph/Opx_{ss}1–5, Table 1) were synthesized following the same procedure but with varying Fe/Mg ratios, as reported in Table 1. The compositions were based on clinopyroxene analyses reported by Yaxley and Brey (2004) from 1,200 °C and were designed to crystallize a significant

proportion of clinopyroxene coexisting with a smaller amount of orthopyroxene or garnet. The results were used to specifically extract clinopyroxene Fe–Mg activity–composition terms.

High-pressure experimental procedure

Experiments at pressures between 4 and 7 GPa were performed in a 1,000-tonne Kawai-type multi-anvil apparatus and in a 500-tonne press equipped with a Walker-type module. An 18/11 (octahedral edge length in mm/anvil corner truncation edge length in mm) octahedral assembly was used as a pressure medium for all experiments. The octahedron was comprised of MgO doped with 5wt% Cr_2O_3 . It was compressed using 8-tungsten carbide anvils of 32-mm edge length.

The OC1/2 starting material was either filled into a graphite capsule with a tight fitting graphite lid or placed into a folded Re foil capsule. These inner capsules were then placed inside an outer platinum tubing capsule (2.0 × 3.5 mm OD), which was welded closed on both sides with an arc welder. Some experiments were also performed using a single $\text{Au}_{80}\text{Pd}_{20}$ capsule (1.2 mm OD/0.9 mm ID or 2.0 mm OD/1.5 mm ID). The different capsule types were employed to examine the influence of variable oxygen fugacity on the calibration.

The variable Fe/Mg starting materials (Omph/Opx_{ss}1–5, Table 1) were loaded into five sample chambers each approximately 0.25 mm in diameter produced in a single Re metal cylinder of 2 mm diameter, by spark erosion. A piece of Re foil was placed over the five holes to chemically isolate the samples from the assembly. Using such multi-chamber capsules, cpx–garnet Fe–Mg partitioning could be studied as a function of Fe/(Fe + Mg) ratio in a single experiment.

All capsule types were placed at the center of a hole drilled inside the octahedral pressure assembly, surrounded by an MgO sleeve, a stepped graphite heater, and a ZrO_2 insulation sleeve. Remaining cavities around the capsule

Table 1 Starting compositions

Oxide	OC1/2	Omph/Opx _{ss} 1	Omph/Opx _{ss} 2	Omph/Opx _{ss} 3	Omph/Opx _{ss} 4	Omph/Opx _{ss} 5
SiO_2	46.5	50.2	49.7	51.2	52.8	54.7
TiO_2	1.0	–	–	–	–	–
Al_2O_3	15.0	6.9	6.9	6.8	6.8	6.7
FeO^a	8.8	27.5	29.6	24.1	17.8	10.8
MnO	0.13	–	–	–	–	–
MgO	8.2	6.0	4.4	8.6	13.3	18.6
CaO	13.6	7.1	7.1	7.0	7.0	6.9
Na_2O	2.5	2.3	2.3	2.3	2.3	2.3
H_2O	2	–	–	–	–	–
F	2	–	–	–	–	–
total	99.7	100	100	100	100	100

^a All Fe given as FeO

Table 2 Experimental run conditions and recovered phases

#	<i>P</i> (GPa)	<i>T</i> _{final} (°C)	<i>T</i> _{start} (°C)	Cooling rate (°C/min)	Runtime (h, min)	Starting material	Capsule	Phases present ^b
A571	3	1,430	1,500	2	3	OC1/2	Graphite	grt, cpx, glass
H3547	4	1,485	1,520	7	3 h 30	OC1/2	Graphite	grt, cpx, glass
H3543	4	1,460	1,500	5	1 h 30	OC1/2	Graphite	grt, cpx
V772-5	4	1,200	1,200	–	24 h	Omph/Opx _{ss}	Re	grt, cpx, glass (not in #5), opx(#5)
V780 ^c	6	1,200	1,200	–	24 h	Omph/Opx _{ss}	Re	grt, cpx, qx (not in #5)
V792 ^c	4	1,050	1,050	–	24 h	Omph/Opx _{ss}	Re	grt, cpx
H3639	5	1,445	1,490	4	1 h 20 min	OC1/2	Au ₈₀ Pd ₂₀	grt, cpx, glass
H3540	6	1,480	1,520	5	1 h 30 min	OC1/2	Re	grt, cpx, glass, qx
H3483	6	1,549 ^a	1,549	–	3 h	OC1/2	graphite	grt, cpx, glass, qx
H3602	6	1,518 ^a	1,518	–	1 h	OC1/2	graphite	grt, cpx, glass
H3510	6	1,430	1,480	5	2 h 8 min	OC1/2	graphite	grt, cpx, coesite
H3605x	7	1,480	1,480	–	1 h 30 min	OC1/2	graphite	grt, cpx

A571 is a piston cylinder experiment, all others are multi-anvil experiments. ^a estimated from the electrical power to the heater

^b grt: garnet, cpx: clinopyroxene, opx: orthopyroxene, qx: quench crystals; ^conly used for obtaining $W_{FeMg}^{M1, CPX}$

were filled with dried MgO powder. The temperature was monitored using D-type thermocouple (W₃Re–W₂₅Re) axially inserted inside an alumina thermocouple tube, with the junction in contact with the top of the sample capsule. A Re disc was inserted between the Pt capsule and the thermocouple to prevent the soft capsule material from being extruded into the thermocouple holes of the alumina tubing, which can cause misleading temperature measurements. No correction for a pressure effect on the thermocouple emf was applied. The experimental pressure was previously calibrated against the quartz–coesite, fayalite (Fe₂SiO₄)–ringwoodite, garnet (CaGeO₃)–perovskite, rutile–TiO₂ II, and coesite–stishovite phase transformations (Keppler and Frost 2005).

Experiments were pressurized for between 1.5–3 h, depending on the final pressure, at room temperature. The run temperature was then raised at ~150 °C/min to approximately 50 °C above the final run temperature. After holding this temperature for 15 min, the sample was cooled to the desired run temperature with a ramp of 2–7 °C/min. The final temperature was held for between 1 and 24 h, depending on the temperature. Some experiments were directly heated to the final temperature (Table 2). The superheating and slow cooling were designed to promote the growth of large homogeneous crystals with a reasonable size for further analytical procedures. The experiments were quenched by switching off the power to the furnace, which caused the temperature to drop to <120 °C in approximately 2 s.

Experiments at lower pressure (3 GPa) were conducted using an end-loaded piston cylinder apparatus. A 1/2" talc-Pyrex tubular pressure medium was employed, containing a tapered graphite heater and Al₂O₃ spacers. A 5.0 × 7.0 mm Pt capsule was used with two different inner sample

containers. One container was made from graphite, while the second was made from folded Re foil. Both capsules were loaded with the same starting material, but should have experienced different oxygen fugacities. The temperature was monitored with a D-type thermocouple.

Recovered capsules from all experiments were embedded in epoxy resin, and then cut and polished with diamond paste. Some capsules were impregnated with epoxy resin under vacuum to fill cavities.

Analytical methods

Run products were examined qualitatively using a Zeiss Gemini 1530 scanning electron microscope (SEM) equipped with a field emission gun and an energy-dispersive X-ray spectrometer (EDXS). Major element concentrations were determined with a 5-spectrometer JEOL JXA-8200 microprobe using an acceleration voltage of 15 kV and a 15 nA beam current. All phases were analyzed with a focused beam. Counting times were 15 s on the peak and 5 s on the background. The following matrix-matched calibration standards were used such as: jadeite (Na), wolastonite (Ca), enstatite (Mg), pyrope (Al), diopside (Si), rutile (Ti), Fe metal (Fe), MnTiO₃ (Mn), Ir metal (Ir), and Re metal (Re). The internal reproducibility was better than 0.5 % for all elements. Mineral analyses which varied by more than 1.5 wt% from 100 wt% totals were neglected.

To evaluate the ferric/ferrous iron ratio in garnet and clinopyroxene, a sample from a graphite/Pt capsule experiment (H3605x) and one from a Re capsule experiment (V772) were examined with a 200-kV Philips CM-20FEG analytical transmission electron microscope (ATEM) equipped with a parallel electron energy-loss spectrometer

(PEELS Gatan 666). The ferric iron over total iron ratio was obtained from the Fe $L_{2,3}$ edge electron energy-loss near-edge structure (ELNES) following the method of van Aken and Liebscher (2002) and van Aken et al. (1998) using the MATLAB™-based software EELSA 1.0 created by C. Prescher. Sample H3605x was ground to a fine powder and placed upon a TEM Cu grid coated with lacey carbon film. Sample V772 was double-polished into a thin section of less than 30- μm thickness, which was glued to a 100-mesh Mo grid. The sample was subsequently thinned to electron transparency by Ar ion milling. A stationary unfocused electron beam with a spot size between 250 and 500 nm was used for EDXS and PEELS. ELNES spectra were collected in diffraction mode with convergence and collection semi-angles of $\alpha = 4$ mrad and $\beta = 2.7$ mrad for sample V772 and $\alpha = 4$ mrad and $\beta = 4.3$ mrad for sample H3605x, an energy dispersion of 0.1 eV per channel and 20- to 40-s integration time per readout. The energy resolution was between 0.8 and 0.9 eV, measured as the full width at half maximum (FWHM) of the zero-loss peak. No oxidation by beam damage was observed, which would have caused a shift in the $\text{Fe}^{3+}/\Sigma\text{Fe}$ ratio during EELS measurements.

Experimental results

Textures and phase relations

Multi-anvil experimental charges from runs employing the hydrous bulk composition OC1/2 (Table 2) yielded euhedral to subhedral garnet and clinopyroxene crystals. Garnet, clinopyroxene, and melt were present in varying proportions in all samples depending on pressure and temperature. Clinopyroxene generally occupies interstitial regions within a relatively coarse-grained garnet matrix. Some samples displayed a layered sequence of minerals and melt between the bottom and the top of the capsule. Depending on temperature and pressure, melt is present as either pale-to-brownish homogeneous glass or as quenched crystals.

Mineral phases are generally transparent. Garnets have a pinkish to yellowish tint, while clinopyroxenes have a greenish tint. The size of the garnets varies between 10 and 500 μm . Clinopyroxenes are elongated and generally smaller, although in some instances were up to 80 μm in the longest dimension. Garnets often contain inclusions of submicron Ir nuggets. Care was taken while analyzing these garnets because large Ir nuggets alloyed with iron can bias the analytical result. Images of typical recovered samples are shown in Fig. 1.

The anhydrous experiments (V772, V780, V792) performed in multi-chamber Re capsules to study Fe–Mg partitioning between 1,050 and 1,200 °C yielded garnet and

clinopyroxene and in some chambers also quenched melt. In addition, orthopyroxene was found in the most Fe-poor capsule chamber. Euhedral garnets are smaller than in the hydrous experiments with sizes not exceeding 20 μm . Clinopyroxenes are subhedral and are up to ~80 μm in the longest dimension. All charges are clearly dominated by clinopyroxene accompanied by less than 5 % garnet. Quenched melt formed at the bottom of the sample chambers and did not exceed 10 % of the chamber volume.

In anhydrous runs where melt was absent, garnets contain slightly iron-enriched cores, whereas these concentric zonations are scarcely observed in experiments where melt was present. Garnet rim analyses were employed in these experiments. Zonations were not observed in clinopyroxenes regardless of whether melt was present and even when very large 80- μm crystals were produced. Quenched melt regions were also observed to be homogeneous throughout the capsules. In all experiments doped with IrO_2 , Ir–Fe alloy was present as small nuggets with a size typically <1–3 μm . Nuggets were generally evenly distributed throughout the capsules, although the bottom and rim of the capsules showed slight accumulations. In Re capsules, Re was additionally present in some alloys.

Run products from piston cylinder experiments generally resembled those from multi-anvil experiments but some twinned clinopyroxenes were produced in addition to some that showed slight zonation. The zoned crystals were treated the same way as described above for the garnets. Generally, the crystalline phases reached significantly larger sizes compared to crystals recovered from multi-anvil experiments, with some crystals growing up to 1 mm in the longest dimension. The crystals are inclusion-free except for small Ir–Fe nuggets.

Mineral chemical compositions

Mineral chemical analyses are presented in Table 3. In melt-bearing experiments, mineral grains were chemically homogeneous and minerals within a single capsule showed very little variation in composition.

Garnet

Garnets are generally dominated by pyrope and grossular components, though in most experiments all three major end members are present in subequal quantities. Garnet grains obtained from the bulk starting material OC1/2, for example, are solid solutions containing between 30 and 34 mol% grossular ($\text{Ca}_3\text{Al}_2\text{Si}_3\text{O}_{12}$), 37–48 mol% pyrope ($\text{Mg}_3\text{Al}_2\text{Si}_3\text{O}_{12}$), and 17–28 mol% almandine ($\text{Fe}_3\text{Al}_2\text{Si}_3\text{O}_{12}$). Minor components of spessartine ($\text{Mn}_3\text{Al}_2\text{Si}_3\text{O}_{12}$; 3–7 mol%), andradite ($\text{Ca}_3\text{Fe}_2^{3+}\text{Si}_3\text{O}_{12}$; up to 5 mol%), majorite ($\text{Mg}_4\text{Si}_4\text{O}_{12}$; up to 5 mol%), and

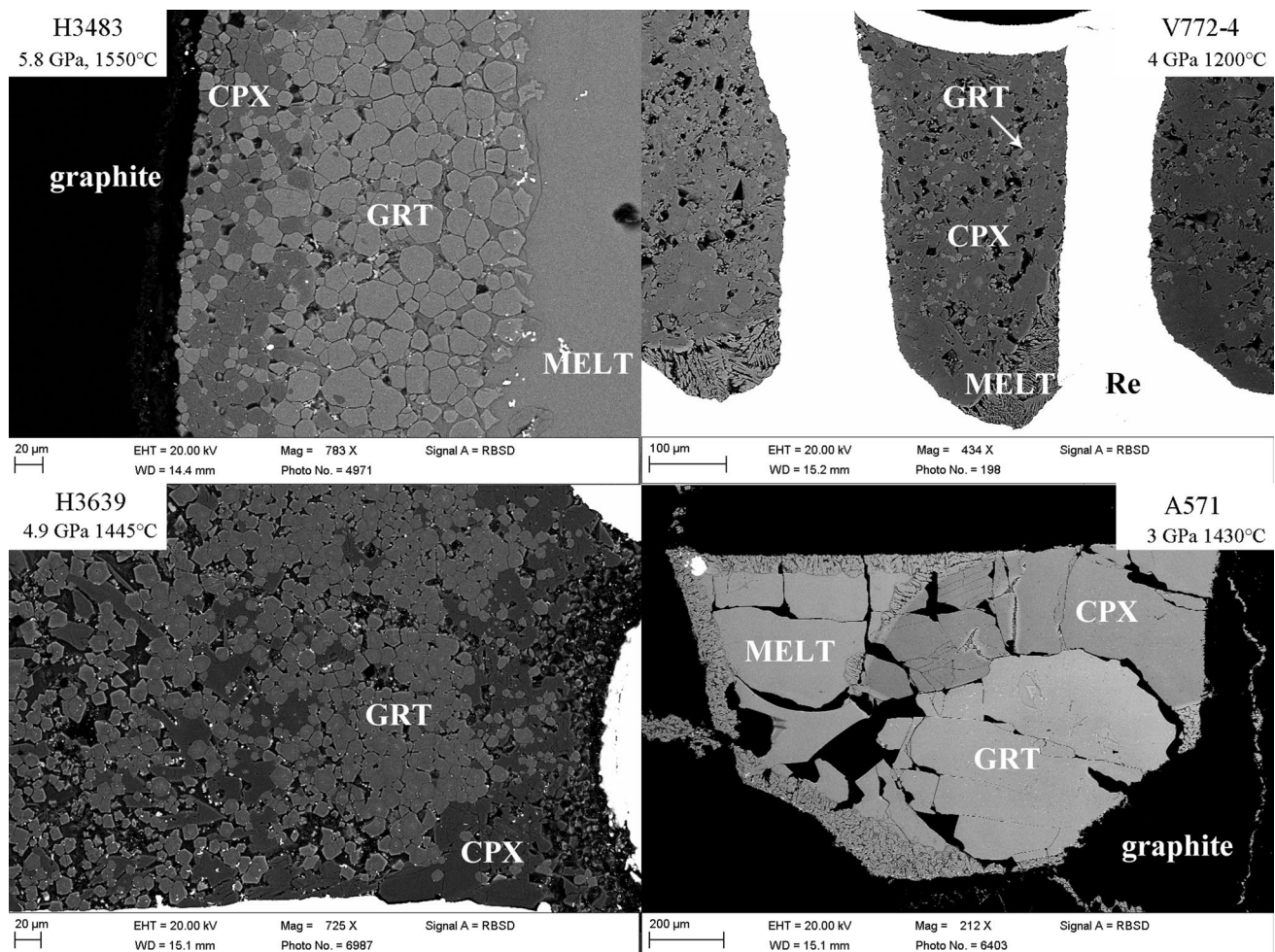


Fig. 1 Representative backscattered electron images of run products from each capsule type (see Table 2 for more details). Experiment H3483 (*top left*) shows vertical banding of cpx-rich material, followed by a garnet-rich band and then glass on going from left to right. The black material on the far left is the graphite capsule. Experiment V772-4 (*top right*) the multi-chamber capsule shows small euhedral garnet grains within a matrix of larger cpx. Quenched

melt can be seen at the base of the chamber. Run H3639 (*bottom left*) shows vertical bands of cpx within garnet and plucked quenched melt on the right-hand side. Piston cylinder experiment A571 (*bottom right*) contains a large garnet crystal at the base with a large (*darker*) cpx crystal above; the *top left* quadrant is occupied by glass. On the capsule rim, the melt formed quench crystals instead of glass

NaTi-garnet ($\text{Na}_2\text{CaTi}_2\text{Si}_3\text{O}_{12}$; ~2 mol%) are also present. Garnets recovered from the anhydrous and more iron-rich bulk compositions (Omph/Op_{ss} 2–5) contain 30–77 mol% almandine, 11–60 mol% pyrope, and 9–13 mol% grossular. NaTi-garnet and majorite component concentrations both show clear positive pressure dependences.

Garnet grains from a graphite capsule experiment (H3605x) performed at 7 GPa and 1,480 °C have $\text{Fe}^{3+}/\Sigma\text{Fe}$ ratios of approximately 0.16 (4). Fe^{2+} may have been oxidized by H_2O in these experiments, with the presence of graphite providing an upper limit to the level of oxidation. This limit depends, however, on the activity of CO_2 in the melt phase, which was not determined. The determined $\text{Fe}^{3+}/\Sigma\text{Fe}$ ratio is similar to recent measurements reported by Purwin et al. (2013) for eclogitic garnets equilibrated in

graphite capsules from 3 GPa and 1,300 °C. Purwin et al. (2013) reported garnet $\text{Fe}^{3+}/\Sigma\text{Fe}$ ratios to increase with temperature above 1,100 °C at 3 GPa and reach 0.15 at 1,300 °C; however, as the presence of graphite does not, on its own, buffer the oxygen fugacity, no direct comparison can be made between the two studies other than noting the qualitative similarity of the measurements.

Garnets analyzed from the anhydrous experiment performed in a Re capsule (V772) at 4 GPa and 1,200 °C have lower $\text{Fe}^{3+}/\Sigma\text{Fe}$ ratios of 0.08 (2). This is slightly lower than the value reported by Purwin et al. (2013) at 3 GPa and 1,200 °C in a graphite capsule but reflects more reducing conditions resulting from the absence of an oxygen source such as H_2O or ReO_2 in the experiments. Since the starting material was reduced at FMQ –2 in the gas-mixing

Table 3 Electron microprobe analyses

Sample:	A571	H3547	H3543	H3540	H3639	H3483	H3602	H3510	H3605x
Conditions [P(GPa)/T (°C)]	3/1430	4/1485	4/1460	6/1480	5/1445	56/1549	6/1518	6/1380	7/1480
Garnet	(10)	(9)	(9)	(17)	(23)	(13)	(6)	(11)	(20)
SiO ₂	40.0 (2)	40.1 (4)	39.9 (3)	40.0 (3)	41.1 (2)	40.6 (5)	40.5 (3)	39.7 (6)	40.1 (2)
TiO ₂	0.4 (1)	0.35 (6)	0.45 (4)	0.4 (1)	0.35 (8)	0.34 (4)	0.52 (9)	0.6 (1)	0.52 (7)
Al ₂ O ₃	22.3 (3)	22.2 (2)	21.8 (2)	21.4 (3)	22.9 (3)	22.1 (2)	21.5 (2)	21.0 (2)	21.6 (1)
FeO*	11.3 (6)	13.3 (4)	14.2 (4)	12.2 (4)	9.2 (9)	11.6 (2)	13.4 (5)	14.3 (3)	14.1 (2)
MgO	12.8 (2)	11.3 (2)	10.7 (3)	11.0 (5)	12.8 (6)	11.7 (2)	10.4 (7)	9.6 (2)	9.9 (2)
MnO	0.29 (4)	0.31 (3)	0.19 (3)	0.25 (3)	0.28 (3)	0.24 (2)	0.26 (2)	0.25 (3)	0.25 (3)
CaO	11.0 (8)	10.9 (3)	10.8 (2)	12.7 (4)	13.0 (5)	12.1 (2)	11.8 (6)	12.3 (2)	12.0 (2)
Na ₂ O	0.12 (2)	0.19 (3)	0.17 (2)	0.28 (3)	0.20 (3)	0.29 (4)	0.27 (3)	0.28 (3)	0.29 (4)
IrO ₂ **	0.2 (2)	0.1 (3)	0.2 (2)	0.2 (2)	0.1 (2)	0.1 (1)	n.m.	0.2 (2)	0.2 (2)
Total	98.6	98.7	98.3	98.4	99.9	99.0	98.5	98.1	98.9
<i>Cations per 12 oxygens</i>									
Si	2.977	3.002	3.008	3.020	2.995	3.013	3.042	3.025	3.017
Ti	0.023	0.020	0.026	0.020	0.019	0.019	0.029	0.034	0.029
Al	1.961	1.957	1.936	1.909	1.968	1.934	1.901	1.879	1.919
Fe	0.668	0.787	0.849	0.731	0.532	0.585	0.795	0.861	0.839
Mg	1.421	1.257	1.207	1.237	1.396	1.293	1.163	1.089	1.111
Mn	0.018	0.020	0.012	0.016	0.017	0.015	0.017	0.016	0.016
Ca	0.881	0.876	0.872	1.024	1.013	0.966	0.046	0.999	0.968
Na	0.017	0.028	0.025	0.041	0.028	0.042	0.039	0.047	0.042
Cation sum	7.961	7.944	7.931	7.998	7.966	7.962	7.931	7.947	7.939
Clinopyroxene	(8) core	(15)	(12)	(16)	(25)	(11)	(8)	(6)	(21)
SiO ₂	49.0 (8)	51.3 (4)	51.8 (3)	53.9 (3)	53.8 (7)	53.4 (2)	53.7 (5)	54.5 (6)	54.9 (2)
TiO ₂	0.37 (7)	0.32 (7)	0.36 (8)	0.16 (3)	0.23 (7)	0.19 (4)	0.5 (4)	0.35 (4)	0.30 (4)
Al ₂ O ₃	13 (1)	13.7 (1)	13.5 (3)	12.4 (2)	12.8 (6)	13.8 (2)	12.7 (4)	12.9 (1)	12.8 (2)
FeO	5.3 (1)	5.5 (1)	5.9 (2)	4.6 (1)	3.4 (5)	4.4 (1)	5.1 (4)	5.0 (2)	5.0 (1)
MgO	10.8 (4)	9.1 (3)	8.8 (3)	8.7 (2)	9.9 (6)	8.7 (1)	8.2 (7)	8.2 (1)	8.2 (1)
MnO	0.10 (1)	0.09 (3)	0.07 (3)	0.05 (2)	0.06 (3)	0.06 (3)	0.05 (1)	0.06 (2)	0.06 (2)
CaO	17.3 (3)	14.6 (1)	14.4 (2)	13.0 (2)	15.0 (3)	12.8 (1)	13.2 (3)	12.9 (1)	12.8 (2)
Na ₂ O	2.45 (9)	3.9 (2)	3.9 (1)	5.6 (1)	4.6 (2)	5.4 (2)	4.9 (2)	5.2 (1)	5.0 (1)
IrO ₂ **	n.m.	n.m.	0.2 (2)	0.1 (1)	0.2 (2)	0.3 (3)	0.2 (3)	0.2 (2)	n.m.
Total	98.9	98.8	98.9	98.5	100.0	99.0	99.16	99.0	99.2
<i>Cations per 6 oxygens</i>									
T									
Si	1.791	1.857	1.874	1.942	1.908	1.916	1.930	1.948	1.958
Al ^{IV}	0.209	0.143	0.126	0.058	0.092	0.084	0.070	0.052	0.042
M2									
Fe ²⁺	0.023	0.025	0.026	0.015	0.010	0.021	0.016	0.019	0.019
Mg	0.105	0.090	0.087	0.062	0.065	0.079	0.057	0.071	0.069
Mn	0.003	0.003	0.002	0.002	0.002	0.002	0.002	0.002	0.002
Ca	0.677	0.568	0.557	0.502	0.571	0.492	0.529	0.493	0.488
Na	0.174	0.274	0.276	0.392	0.316	0.378	0.341	0.356	0.348
M1									
Al ^{VI}	0.366	0.446	0.451	0.470	0.444	0.501	0.467	0.476	0.495
Ti	0.010	0.010	0.010	0.004	0.008	0.005	0.013	0.010	0.008
Fe ³⁺ (+)	0.032	0.034	0.035	0.009 [‡]	0.020	0.024	0.030	0.030	0.029

Table 3 continued

Clinopyroxene	(8) core	(15)	(12)	(16)	(25)	(11)	(8)	(6)	(21)		
Fe ²⁺	0.107	0.111	0.116	0.095	0.071	0.103	0.107	0.102	0.101		
Mg	0.484	0.399	0.388	0.403	0.457	0.385	0.382	0.382	0.367		
Cation sum	3.982	3.959	3.948	3.972	3.964	3.973	3.944	3.941	3.925		
Sample	V772-2	V772-3	V772-4	V772-5	V780-1	V780-2	V780-3	V780-4	V780-5	V792-4	V792-5
Conditions (P [GPa]/T [°C])	4/1200	4/1200	4/1200	4/1200	6/1200	6/1200	6/1200	6/1200	6/1200	4/1050	4/1050
Garnet	(6)	(7)	(8)	(7)	(7)	(10)	(9)	(10)	(10)	(5)	(5)
SiO ₂	38.0 (3)	38.8 (1)	40.2 (4)	42.4 (4)	38.3 (2)	38.8 (2)	39.4 (2)	41.0 (6)	41.4 (2)	40.3 (2)	41.2 (4)
TiO ₂	n.m.	n.m.	n.m.	n.m.	n.m.	n.m.	n.m.	n.m.	n.m.	n.m.	n.m.
Al ₂ O ₃	20.4 (4)	21.3 (1)	21.7 (3)	22.8 (6)	19.9 (4)	20.4 (4)	21.1 (2)	21.7 (6)	22.2 (2)	21.6 (3)	21.7 (5)
FeO*	34.4 (5)	30.2 (3)	25.0 (9)	14.9 (6)	35.4 (3)	34.0 (3)	29.6 (2)	22.5 (3)	19.0 (8)	25 (1)	17.8 (2)
MgO	2.9 (1)	6.0 (1)	9.7 (4)	16.9 (9)	3.3 (1)	4.01 (8)	7.2 (1)	12.2 (4)	14.6 (4)	9.7 (8)	15.2 (2)
MnO	n.m.	n.m.	n.m.	n.m.	n.m.	n.m.	n.m.	n.m.	n.m.	n.m.	n.m.
CaO	4.9 (4)	4.2 (2)	4.3 (4)	3.8 (7)	3.9 (1)	3.8 (1)	3.7 (3)	3.7 (4)	3.3 (3)	4.9 (8)	4.6 (2)
Na ₂ O	0.06 (3)	0.06 (3)	0.07 (5)	0.09 (8)	0.16 (2)	0.14 (2)	0.12 (3)	0.15 (7)	0.11 (1)	0.08 (5)	0.3 (1)
IrO ₂ **	n.m.	n.m.	n.m.	n.m.	n.m.	n.m.	n.m.	n.m.	n.m.	n.m.	n.m.
Total	100.7	100.6	100.9	100.8	100.9	101.1	101.1	101.3	100.6	101.6	100.8
<i>Cations per 12 oxygens</i>											
Si	3.015	3.008	3.023	3.040	3.055	3.055	3.035	3.047	3.042	3.031	3.022
Ti											
Al	1.905	1.942	1.925	1.930	1.867	1.893	1.918	1.902	1.922	1.912	1.879
Fe	2.280	1.956	1.573	0.893	2.356	2.244	1.908	1.399	1.169	1.582	1.093
Mg	0.343	0.696	1.090	1.903	0.387	0.471	0.828	1.351	1.595	1.089	1.663
Mn											
Ca	0.405	0.347	0.345	0.291	0.333	0.324	0.308	0.294	0.262	0.393	0.360
Na	0.011	0.009	0.010	0.013	0.025	0.021	0.018	0.022	0.016	0.012	0.040
Cation sum	7.959	7.958	7.966	7.970	8.024	8.009	8.015	8.013	8.005	8.019	8.058
Clinopyrox-(12)ene	(12)	(11)	(11)	(16)	(18)	(22)	(14)	(19)	(5)	(3)	
SiO ₂	50.4 (2)	51.9 (2)	53.4 (2)	55.5 (2)	50.8 (2)	51.3 (3)	52.5 (2)	54.4 (2)	55.0 (3)	51.6 (6)	53.7 (3)
TiO ₂	n.m.	n.m.	n.m.	n.m.	n.m.	n.m.	n.m.	n.m.	n.m.	n.m.	n.m.
Al ₂ O ₃	4.3 (3)	4.5 (4)	5.3 (2)	5.4 (4)	4.0 (4)	4.2 (5)	4.8 (3)	7.6 (8)	7.7 (2)	7 (1)	6.4 (2)
FeO	31.0 (9)	24.3 (5)	18.1 (4)	9.3 (8)	31 (2)	29 (1)	22 (1)	16 (1)	12.3 (6)	17.9 (4)	10.0 (3)
MgO	5.0 (1)	9.6 (2)	13.2 (2)	18.2 (6)	5.3 (2)	6.8 (5)	10.1 (4)	15.0 (6)	17.9 (5)	12.8 (6)	15.8 (4)
MnO	n.m.	n.m.	n.m.	n.m.	n.m.	n.m.	n.m.	n.m.	n.m.	n.m.	n.m.
CaO	7.2 (4)	7.3 (3)	7.6 (2)	8.9 (8)	7.3 (6)	7.3 (7)	7.8 (5)	7.6 (8)	7.7 (2)	8.5 (4)	10.4 (6)
Na ₂ O	2.5 (1)	2.3 (2)	2.5 (1)	2.8 (2)	2.6 (3)	2.7 (3)	2.9 (2)	2.7 (3)	2.62 (9)	2.9 (2)	3.6 (1)
IrO ₂ **	n.m.	n.m.	n.m.	n.m.	n.m.	n.m.	n.m.	n.m.	n.m.	n.m.	n.m.
total	100.4	100.1	100.0	100.1	100.9	100.7	100.4	100.8	100.3	100.2	99.9
<i>Cations per 6 oxygens</i>											
T											
Si	1.979	1.977	1.976	1.972	1.997	1.995	1.989	1.988	1.985	1.803	1.771
Al ^{IV}	0.021	0.023	0.024	0.028	0.003	0.005	0.011	0.012	0.015	0.197	0.229
M2											
Fe ²⁺	0.368	0.289	0.205	0.091	0.388	0.355	0.267	0.195	0.146	0.228	0.115
Mg	0.116	0.219	0.291	0.344	0.118	0.151	0.216	0.319	0.378	0.289	0.325
Mn											

Table 3 continued

Clinopyrox-ene	(12)	(11)	(11)	(16)	(18)	(22)	(14)	(19)	(5)	(3)
Ca	0.302	0.296	0.300	0.375	0.306	0.303	0.317	0.297	0.297	0.366
Na	0.191	0.172	0.180	0.191	0.199	0.200	0.209	0.192	0.183	0.228
M1										
Al ^{VI}	0.179	0.181	0.207	0.196	0.181	0.186	0.202	0.199	0.189	0.329
Ti										
Fe ³⁺ (+)	0.080 [‡]	0.061 [‡]	0.044 [‡]	0.022 [‡]	0.080 [‡]	0.073 [‡]	0.056 [‡]	0.039 [‡]	0.029 [‡]	0.073 [‡]
Fe ²⁺	0.564	0.430	0.310	0.163	0.628	0.572	0.442	0.303	0.226	0.295
Mg	0.177	0.327	0.440	0.620	0.191	0.186	0.202	0.199	0.189	0.453
Cation sum	3.977	3.976	3.977	4.001	4.011	4.009	4.009	4.002	4.005	4.035

Number of analyses is given in parentheses at the head of each column. Number in parentheses after each analysis is the standard deviation in terms of least units cited. *All Fe is reported as FeO. **Ir nuggets were present as small inclusions (<1 μm). (+) Fe³⁺/ΣFe ratios taken from EELS measurements on the two samples from different capsules. (‡) Fe³⁺/ΣFe for cpx is 0.06 and for all other samples 0.19. *n.m.* not measured

furnace and there was no oxygen source, the oxygen fugacity likely remained at a similar level.

The obtained Fe³⁺/ΣFe ratios have been used in Table 3 to calculate cation proportions of both ferric and ferrous iron in garnet, with the ratios assumed to be identical in all samples employing the same type of capsule. However, in the following discussion and in all thermodynamic calculations, garnet end members have been calculated by assuming all Fe analyzed is Fe²⁺ to allow applicability to data sets with unknown Fe³⁺ concentrations. The proportion of the grossular component in garnet is, therefore, defined as the Ca mole fraction on the dodecahedral site, i.e.,

$$X_{Ca} = \left[\frac{Ca}{(Ca + Mg + Fe^{total})} \right] \quad (2)$$

with similar expressions for X_{Mg} and X_{Fe}. Mixing on the Al and Si sites in garnet were neglected in modelling.

Clinopyroxene

The eclogitic clinopyroxenes can be considered to be multisite solid solutions with the general formula (Fe, Ca, Na, Mg)^{M2}(Fe, Mg, Al, □)^{M1}(Si, Al)^{IV}Si^{IV}O₆ (Mukhopadhyay 1991; Simakov 2008). Clinopyroxenes analyzed from a hydrous experiment (H3605x) performed in a graphite capsule at 7 GPa and 1,480 °C yielded Fe³⁺/ΣFe ratios of 0.19(3) (Fig. 2), although the absolute uncertainty on the measurement is in the range 15–30 % due to the low total Fe concentration, which is close to the resolution limit of the EELS system. This ratio is similar to values reported for eclogitic clinopyroxenes formed in graphite capsules by Purwin et al. (2013) at 3 GPa but only at temperatures below 1,200 °C. At higher temperatures, Purwin et al. (2013) report a steep drop in clinopyroxene Fe³⁺/ΣFe ratios. Clinopyroxenes from Re capsule experiments at

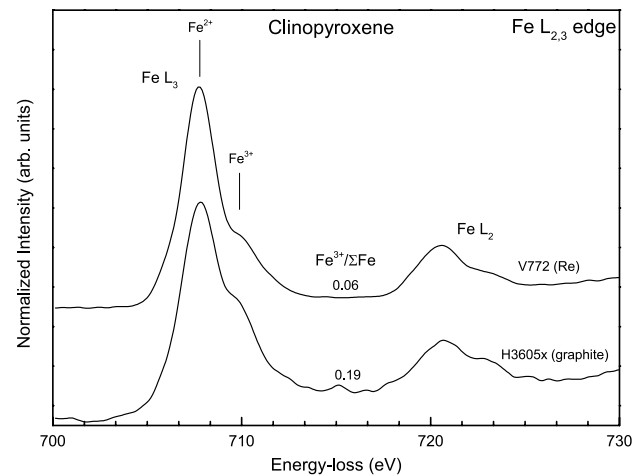


Fig. 2 Normalized and deconvoluted EELS spectra of clinopyroxenes from sample H3605x (graphite capsule) and V772 (Re capsule). The Fe³⁺/ΣFe ratios were determined following the method of van Aken et al. (1998)

4 GPa and 1,200 °C yielded Fe³⁺/ΣFe ratios of 0.06 (1), which are much lower than the measurements of Purwin et al. (2013) from the same temperature.

To calculate the proportion of cpx end members, the method of Zhao et al. (2011) has been applied, and the following end members considered jadeite (NaAlSi₂O₆), diopside/hedenbergite (Ca{Mg,Fe}Si₂O₆), enstatite/ferrosilite ({Mg,Fe}₂Si₂O₆), Ca-Tschermaks (CaAlAlSiO₆), and Ca-Eskola (Ca_{0.5-0.5}AlSi₂O₆). Ferric iron could be assigned to either an acmite (NaFeSi₂O₆) or a CaFeAlSiO₆ component, but has been ignored in modelling of the barometer for the same reasons as described above for garnet. Furthermore, as the total amount of Fe³⁺, as shown in Table 3, is small, it most likely has no major effect on equilibrium 1. The following site assignments are made, starting with

the determination of the proportion of tetrahedrally coordinated Al, which also defines the proportion of the Ca-Tschermaks (CaTs) component

$$Al^{IV} = 2 - Si \tag{3}$$

where Si is, for example, the number of Si atoms per 6 oxygen formula units. The remaining Al is assigned to the M1 site,

$$Al^{M1} = Al - Al^{IV} \tag{4}$$

A portion of this remaining Al is then assigned to jadeite, i.e.,

$$Jadeite (NaAlSi_2O_6) = Na \tag{5}$$

Although not important for the barometry calculations described later, any remaining Al is assumed to form the Ca-Eskola component, determined from

$$Ca \text{ Eskola} = Al - 2Al^{IV} - Na. \tag{6}$$

where Ca, Na, and Mn are assigned to the M2 site. Mg, Fe, and Ti are assigned to M1 until the site occupancy is 1, upon which the residual Mg + Fe is assigned to M2. The Fe/(Fe + Mg) ratio in both M1 and M2 sites is constrained to be the same. Fe³⁺ contents in the cpx M1 site are shown in Table 3, calculated by assuming Fe³⁺/ΣFe ratios are the same for each capsule type as in the two representative samples examined. As stated previously, however, all Fe is considered to be Fe²⁺ in the barometer refinement. Although this does influence the calculated proportion of Ca-Eskola, the mixing of Ca-Eskola-associated vacancies on M2 is anyway ignored in the thermodynamic modelling so this should have no implications.

These site assignments result in clinopyroxene compositions for starting material OC1/2 with 17–38 mol% jadeite, 27–37 mol% diopside/hedenbergite, 7–13 mol% (clino-)enstatite/ferrosilite, 7–20 mol% Ca-Tschermaks, and 0–10 mol % Ca-Eskola. The anhydrous starting materials Omph/Op_{x_{ss}} yielded clinopyroxenes with 17–19 mol% jadeite, 30–38 mol% diopside/hedenbergite, 44–51 mol% (clino-)enstatite/ferrosilite, 2–3 mol% Ca-Tschermaks, and <1 mol% Ca-Eskola.

An alternative procedure for clinopyroxene component assignment is to first determine the proportion of Ca-Eskola from the deficit in the total number of cations compared to the four cations in the formula (Pertermann and Hirschmann 2003). Further components are then assigned in the reverse order to those used in this study. The different procedures result in quite different assignments, particularly for Ca-Eskola, in some instances. These differences arise because the techniques are sensitive to different uncertainties in the microprobe measurements. The

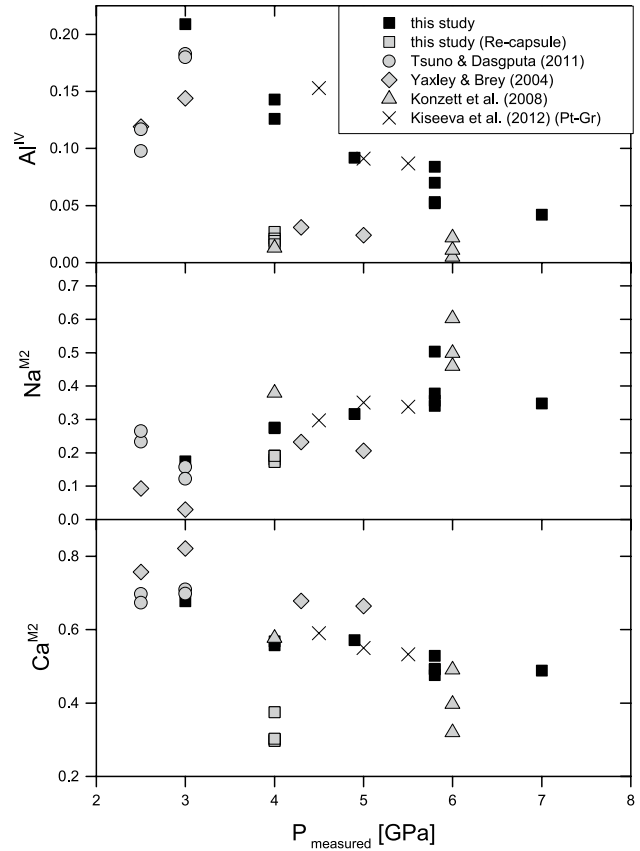


Fig. 3 Clinopyroxene cation contents, in terms of a 6 oxygen formula unit, plotted as a function of pressure. The data are from various temperatures, which causes the main variation other than pressure. Pt-Gr means platinum-graphite capsule. Re capsule experiments from this study were performed at 1,200 °C, while the other experiments from this study were performed in the range 1,377–1,550 °C. For clarity, only the results of Kiseeva et al. (2012) collected at 1,250 °C are shown

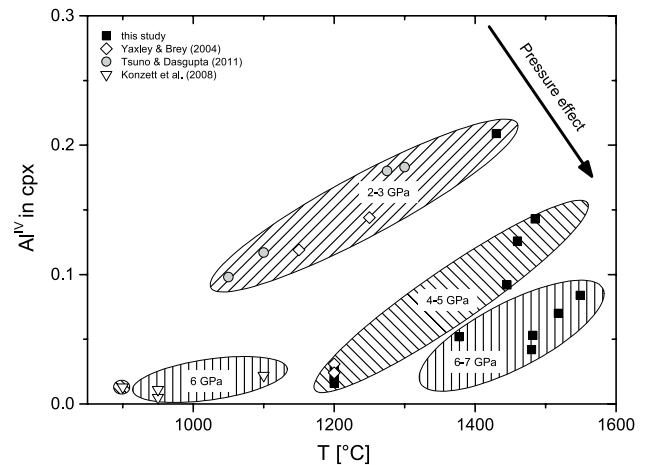


Fig. 4 Variation with temperature of the clinopyroxene tetrahedral Al concentration (Al^{IV}) in formula units. Pressures are indicated by the banded areas

method employed here results in a smaller uncertainty in the Al^{IV} content, which is then not influenced by the error in the Fe³⁺/ΣFe ratio and uncertainties over the proportion of ferric iron components. When employing clinopyroxene data from previous studies, component assignments have been redetermined, where necessary, to be consistent with the method used here.

Figure 3 shows how the clinopyroxene Al^{IV} component decreases with pressure between 3 and 7 GPa in line with previous studies (Kiseeva et al. 2012; Klemme et al. 2002; Pertermann and Hirschmann 2003). The Na, i.e., jadeite component, on the other hand, increases with pressure. This reflects an exchange of Al between the tetrahedrally coordinated Si site and octahedrally coordinated M1 site, which leaves the total clinopyroxene Al content relatively constant with pressure at a given temperature. The Al^{IV} content also increases with temperature (Fig. 4) while the proportion of the jadeite component decreases with temperature. The combined effect is an increase in the total cpx Al content with temperature, as reported by Kiseeva et al. (2012). In comparison with the study of Kiseeva et al. (2012), however, cpx Al^{IV} contents measured at a similar pressure and temperature in this study are systematically lower, as will be discussed later. The cpx Ca content increases with temperature and decreases with pressure. This is matched by a corresponding increase in the garnet Ca content with pressure.

Melt analyses

The melt phase is present either as homogeneous glass or as small quenched dendritic crystals. When both glass and dendrites are present, the quench crystals preferentially crystallized on the contact between sample and capsule material. When a large fraction of melt is present (>~20 vol.%), the melt tends to form a glass, whereas smaller melt fractions crystallize as dendritic quench crystals. The amount of quenched melt increased with increasing temperature at the expense of clinopyroxene. At higher pressures, the proportion of melt decreases at a given temperature. The chemical composition of the glass and the quench crystals is virtually identical throughout the samples with variations only in SiO₂, which appears to be 2–4 wt% higher in the quenched crystals. The glass/quench crystals of starting material OC1/2 are basaltic melts with 46–50 wt% SiO₂ and 1.4–3.5 wt% Na₂O. The analytical sums were generally below 98 wt% indicating high contents of volatile components, i.e., F and H₂O. Measurements of F in the glass gave F concentrations between 1 and 3.9 wt%, depending on the melt fraction.

Quenched melts recovered from the anhydrous experiment V772 (Omph/Opx_{ss} 2-4) are also basaltic with SiO₂ concentrations of 49–53 wt% and Na₂O concentrations of

2.4–3.3 wt%. The melt FeO content varies strongly, from 9 to 35 wt%, due to the significantly different bulk FeO/MgO ratios of the starting materials. The fraction of melt decreases with decreasing bulk FeO content in the samples, and melt is absent in the chamber with the lowest bulk FeO content (V772-5).

Attainment of equilibrium

The attainment of equilibrium is critical to the accuracy of the geobarometer calibration because it relies on the cpx Al concentration, which can be strongly zoned if equilibrium is not obtained. In the current experiments, the presence of a significant proportion of hydrous silicate melt acted as a flux from which mineral grains were crystallized. This was aided by initially raising the temperature by 50 °C in the first 15 min of the experiment and then cooling to the run temperature. Crystals that grow from the melt show very little chemical zonation, and crystals throughout the charge have a homogeneous composition, even though some are up to 0.3 mm in diameter, which is good evidence for the attainment of equilibrium.

A further method for assessing the state of equilibrium is to obtain an independent estimate for the temperature of the experiments using the Ellis and Green (1979) and Nakamura (2009) garnet–clinopyroxene geothermometer, which is a sensitive function of the Fe–Mg exchange between the mineral phases. Such estimates are compared with the thermocouple temperature in Fig. 5. Given the likely thermal gradient throughout the charge (~50 °C), the uncertainty of ±50 °C for both geothermometers and accounting for the uncertainty in the electron microprobe analyses, acceptable levels of equilibrium should give temperatures within 100 °C of the thermocouple temperature. The majority of samples plot within a mean deviation of ±32 °C. Experiments that fell outside of the ±100 °C range were excluded.

Thermodynamic model

Equilibrium (1) describes the distribution of Al₂O₃ between garnet and clinopyroxene. If pressure and temperature influences on the volume are ignored, then at equilibrium pressure can be determined from the expression

$$P = - \left[\Delta G_{T,1\text{bar}}^0 + RT \ln K_{(1)} \right] / \Delta V_r \quad (7)$$

where R is the gas constant and $\Delta G_{T,1\text{bar}}^0$, ΔV_r , and $K_{(1)}$ are the standard state Gibbs free energy change, (with the standard state being the pure phases at 1 bar and the temperature of interest), molar volume change in the pure phases and the equilibrium constant of reaction (1), respectively. $\Delta G_{T,1\text{bar}}^0$ and ΔV_r can be calculated from end-member thermodynamic data (Holland and Powell 2011), and

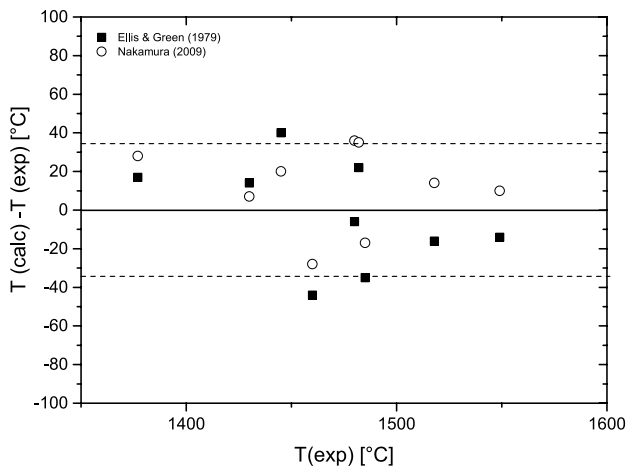


Fig. 5 Difference between experimental thermocouple temperatures and the temperature calculated with the Ellis and Green (1979) and Nakamura (2009) geothermometers for experiments performed in this study

over the range of plausible eclogite equilibration conditions, i.e., 2–7 GPa and 700–1,400 °C, the calculated values can be fitted by the simple expression

$$\Delta G_{T,1bar}^0 = 16500 - 23.50 * T \tag{8}$$

with

$$\Delta V_r = 0.719 \text{ J/bar} \tag{9}$$

being a suitable average value applicable over the range of conditions. The equilibrium constant for equilibrium (1) is

$$K_{(1)} = \frac{a_{Di}^{Cpx} a_{CaTs}^{Cpx}}{[a_{Gr}^{Gt}]^{2/3} [a_{Py}^{Gt}]^{1/3}} = \frac{X_{Di}^{Cpx} X_{CaTs}^{Cpx}}{[X_{Gr}^{Gt}]^{2/3} [X_{Py}^{Gt}]^{1/3}} \cdot \frac{\gamma_{Di}^{Cpx} \gamma_{CaTs}^{Cpx}}{[\gamma_{Gr}^{Gt}]^{2/3} [\gamma_{Py}^{Gt}]^{1/3}} \tag{10}$$

where *a*, *X*, and γ refer to the activity, molecular fraction, and activity coefficient of the mineral components. Rearranging Eq. (7) gives an expression for $\Delta G_{T,P}^0$ the standard state Gibbs free energy at the pressure and temperature of interest, i.e.,

$$\Delta G_{T,1bar}^0 + P\Delta V_r = -RT \ln K_{(1)} \tag{11}$$

The barometer is calibrated by minimizing the difference between both sides of this equation for each experimental data point. To do this, most of the required thermodynamic data have been taken from the literature and in particular from studies that have determined thermodynamic parameters using large experimental data sets (e.g.,

Ganguly et al. 1996; Holland and Powell 2011). Only the less well-constrained activity–composition relationships for clinopyroxene have been refined using the experimental results and some results from previous studies. $K_{(1)}$ is determined from the mineral compositions using Eq. (10) as follows. For garnet, mixing is considered only on the dodecahedral site, with the molecular fractions of the garnet components defined as

$$X_{Gr}^{Gt} = (X_{Ca})^3 \tag{12}$$

and

$$X_{Py}^{Gt} = (X_{Mg})^3 \tag{13}$$

The activity coefficients are described using an asymmetric Margules model

$$RT \ln \gamma_{Gr}^{Gt} = 0.5W_{CaMg}X_{Mg}[1 - X_{Ca} + X_{Mg} + 2X_{Ca}(X_{Ca} - X_{Mg} - 1)] + 0.5W_{MgCa}X_{Mg}[1 - X_{Ca} - X_{Mg} - 2X_{Ca}(X_{Ca} - X_{Mg} - 1)] + 0.5W_{CaFe}X_{Fe}[1 - X_{Ca} + X_{Fe} + 2X_{Ca}(X_{Ca} - X_{Fe} - 1)] + 0.5W_{FeCa}X_{Fe}[1 - X_{Ca} - X_{Fe} - 2X_{Ca}(X_{Ca} - X_{Fe} - 1)] + W_{MgFe}X_{Mg}X_{Fe}(X_{Mg} - X_{Fe} - 0.5) + W_{FeMg}X_{Fe}X_{Mg}(X_{Fe} - X_{Mg} - 0.5) + W_{CaMgFe}X_{Mg}X_{Fe}(1 - 2X_{Ca}) \tag{14}$$

$$RT \ln \gamma_{Py}^{Gt} = 0.5W_{MgCa}X_{Ca}[1 - X_{Mg} + X_{Ca} + 2X_{Mg}(X_{Mg} - X_{Ca} - 1)] + 0.5W_{CaMg}X_{Mg}[1 - X_{Mg} - X_{Ca} - 2X_{Mg}(X_{Ca} - X_{Mg} - 1)] + 0.5W_{MgFe}X_{Fe}[1 - X_{Mg} + X_{Fe} + 2X_{Mg}(X_{Mg} - X_{Fe} - 1)] + 0.5W_{FeMg}X_{Mg}[1 - X_{Mg} - X_{Fe} - 2X_{Mg}(X_{Mg} - X_{Fe} - 1)] + W_{CaFe}X_{Ca}X_{Fe}(X_{Ca} - X_{Fe} - 0.5) + W_{FeCa}X_{Fe}X_{Ca}(X_{Fe} - X_{Ca} - 0.5) + W_{CaMgFe}X_{Ca}X_{Fe}(1 - 2X_{Mg}) \tag{15}$$

Garnet Margules parameters (*W*) are well constrained over wide ranges of composition by a large number of previous experimental data. To take advantage of this, values were taken from the model derived by Ganguly et al. (1996). The relatively small pressure-dependent terms arising from the excess volumes of mixing were neglected to avoid the necessity to iterate the barometer Eq. (2) in terms of pressure. Garnet Margules parameters are given in Table 4 on a single-site basis, i.e., Eqs. (14) and (15) must be multiplied by 3.

For clinopyroxene, mixing occurs on four sites (Simakov 2008; Wood and Banno 1973) with thermodynamic molecular fractions employed in Eq. (10) defined by

$$X_{Di}^{Cpx} = X_{Ca}^{M2} X_{Mg}^{M1} (X_{Si}^{IV})^2 \tag{16}$$

Table 4 Interaction parameters for garnet and clinopyroxene

Parameter (W_{ij})	Garnet	Clinopyroxene		
	X^a	M1	M2	T
W_{CaMg}	21.6–0.00578T		24.9	
W_{MgCa}	9.8–0.00578T			
W_{CaFe}	0.87–0.00169T		–49.3	
W_{FeCa}	0.68–0.00169T			
W_{MgFe}	2.1			
W_{FeMg}	0.7	0	0	
W_{MgAl}		4.9		
W_{FeAl}		3.6		
W_{CaNa}			11.6	
W_{MgNa}			–35.9	
W_{FeNa}			59.3	
W_{AlSi}				7.0

All values reported on a single-site bases and in kJ/mol. T in K. ^aData compiled by Ganguly et al. (1996), P-dependent terms set to zero. The ternary interaction term is calculated from $W_{CaMgFe} = [(W_{MgCa} - W_{CaMg}) + (W_{CaFe} - W_{FeCa}) + (W_{FeMg} - W_{MgFe})]/2$

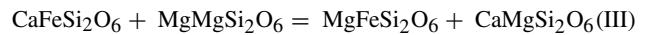
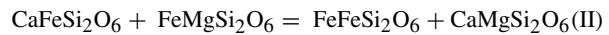
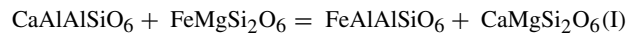
$$X_{CaTs}^{Cpx} = 4X_{Ca}^{M2}X_{Al}^{M1}X_{Al}^{IV}X_{Si}^{IV} \tag{17}$$

where $X_{Al}^{IV} = Al^{IV}/2$, Al^{IV} is as defined in Eq. (3) and $X_{Si}^{IV} = Si/2$. The remaining site mole fractions are determined as described above. Activity coefficients were calculated assuming a ternary symmetric mixing model for the M1 site and a quaternary symmetric mixing model for the M2 site. For the tetrahedral site, a simple binary mixing model is introduced to account for Al^{IV} –Si interaction. This gives the following activity models for clinopyroxene:

$$\begin{aligned}
 RT \ln \gamma_{Di} &= \left[W_{MgAl}X_{Al}^2 + W_{MgFe}X_{Fe}^2 + X_{Fe}X_{Al}(W_{MgFe} + W_{MgAl} - W_{FeAl}) \right]^{[M1]} \\
 &+ [W_{CaMg}X_{Mg}^2 + W_{CaNa}X_{Na}^2 + W_{CaFe}X_{Fe}^2 + X_{Mg}X_{Fe}(W_{CaMg} + W_{CaFe} - W_{MgFe}) \\
 &+ X_{Mg}X_{Na}(W_{CaMg} + W_{CaNa} - W_{MgNa}) + X_{Na}X_{Fe}(W_{CaNa} + W_{CaFe} - W_{NaFe})]^{[M2]} \\
 &+ (W_{AlSi}X_{Al}^2)^{[IV]}
 \end{aligned} \tag{18}$$

$$\begin{aligned}
 RT \ln \gamma_{CaTs} &= \left[W_{MgAl}X_{Mg}^2 + W_{FeAl}X_{Fe}^2 + X_{Mg}X_{Fe}(W_{MgAl} + W_{FeAl} - W_{MgFe}) \right]^{[M1]} \\
 &+ [W_{CaMg}X_{Mg}^2 + W_{CaNa}X_{Na}^2 + W_{CaFe}X_{Fe}^2 + X_{Mg}X_{Fe}(W_{CaMg} + W_{CaFe} - W_{MgFe}) \\
 &+ X_{Mg}X_{Na}(W_{CaMg} + W_{CaNa} - W_{MgNa}) + X_{Na}X_{Fe}(W_{CaNa} + W_{CaFe} - W_{NaFe})]^{[M2]} \\
 &+ (W_{AlSi}X_{Si}^2)^{[IV]}
 \end{aligned} \tag{19}$$

To account for the interaction between cations from different sites, the following reciprocal equilibria were examined (Mukhopadhyay 1991; Simakov 2008; Wood and Nicholls 1978):



With the following Gibbs free energies, $\Delta G_I^0 = -21$ kJ, $\Delta G_{II}^0 = -4.68$ kJ, $\Delta G_{III}^0 = -5.01$ kJ (Mukhopadhyay 1991). The following reciprocal terms should then be added to the activity–composition formulations of diopside and CaTs:

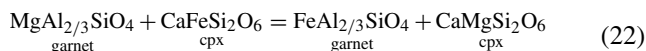
$$\begin{aligned}
 RT \ln \gamma_{CaTs}(\text{Recip}) &= (1 - X_{Al}^{M1})(X_{Fe}^{M2} \Delta G_I^0) \\
 &- X_{Fe}^{M1}(X_{Fe}^{M2} \Delta G_{II}^0 + X_{Mg}^{M2} \Delta G_{III}^0)
 \end{aligned} \tag{20}$$

$$\begin{aligned}
 RT \ln \gamma_{Di}(\text{Recip}) &= -X_{Al}^{M1}(X_{Fe}^{M2} \Delta G_I^0) \\
 &- X_{Fe}^{M1}(X_{Fe}^{M2} \Delta G_{II}^0 + X_{Mg}^{M2} \Delta G_{III}^0)
 \end{aligned} \tag{21}$$

For the experimental eclogite data tested, however, these expressions make contributions to the total free energy that are generally <1 kJ, which makes them trivial in comparison with the interaction terms of the individual clinopyroxene sites (Table 4). The magnitude of these terms increases mainly with the Mg and Fe proportion on the M2 site; however, as most experimental and natural samples have <0.2 formula units of Mg + Fe on M2, these terms can be safely neglected.

Using the results of experiments V772, V780, and V792 (Table 2), which employed multi-chamber capsules and

each contained a range of starting materials with different Fe/Mg ratios, it was possible to obtain an estimate of the $W_{\text{MgFe}}^{\text{Cpx}}$ interaction term that is independent from the rest of the experimental data. The five bulk starting materials in each capsule covered Mg/Fe ratios from ~0.2 to ~0.8. The Mg–Fe exchange between garnet and clinopyroxene can be described with the following equilibrium on a single-site basis



from this, the following distribution coefficient K_D is obtained as:

$$K_D = \frac{X_{\text{Mg}}^{\text{Cpx}} X_{\text{Fe}}^{\text{Gt}}}{X_{\text{Mg}}^{\text{Gt}} X_{\text{Fe}}^{\text{Cpx}}} \quad (23)$$

To calculate the interaction term describing Mg–Fe mixing in clinopyroxene, i.e., $W_{\text{MgFe}}^{\text{Cpx}}$, both garnet and cpx sites are considered to be symmetric solid solutions, which results in the following expression for K_D

$$RT \ln K_D = -\Delta G^0 + W_{\text{FeMg}}^{\text{Gt}} (2X_{\text{Fe}}^{\text{Gt}} - 1) + W_{\text{FeMg}}^{\text{Cpx}} (1 - 2X_{\text{Fe}}^{\text{Cpx}}) \quad (24)$$

This expression was then fitted to the experimental data using a least squares routine where ΔG^0 and $W_{\text{FeMg}}^{\text{Cpx}}$ were refined parameters and the term $W_{\text{FeMg}}^{\text{Gt}}$, which has been well studied, was calculated from the model of Ganguly et al. (1996) at the appropriate garnet Ca concentration. A comparison between the fitted terms in Eq. (24) and the experimental K_D for each experiment is shown in Fig. 6. The resulting value for $W_{\text{FeMg}}^{\text{Cpx}}$ is -360 J/mol with an average deviation from the fit of less than 1 kJ. Although this fitting procedure assumes single-site mixing for Fe and Mg in cpx, as the interaction parameter obtained is essentially zero, Fe–Mg mixing terms on both M1 and M2 are assumed to be zero in the following model.

Each experimental data point was then used to calculate the difference across Eq. (11), and these differences were minimized using a least squares procedure, by refining the clinopyroxene Margules terms in Eqs. (18) and (19). Two terms for the clinopyroxene M1 site were refined, five for M2 and one describing Si–Al interaction. To expand the range of conditions and compositions covered in this refinement, further literature studies were employed. A criterion for the use of previous studies was that they employed eclogitic bulk compositions, covered conditions where a detectable clinopyroxene CaTs component was present, and that high-quality mineral chemical analyses were provided with small analytical standard deviations. Experiments where heterogeneous mineral compositions led to large Al and Si standard deviations were neglected. In addition, all data were tested using the Ellis and Green (1979) and Nakamura (2009) garnet–clinopyroxene geothermometer, and any data that failed

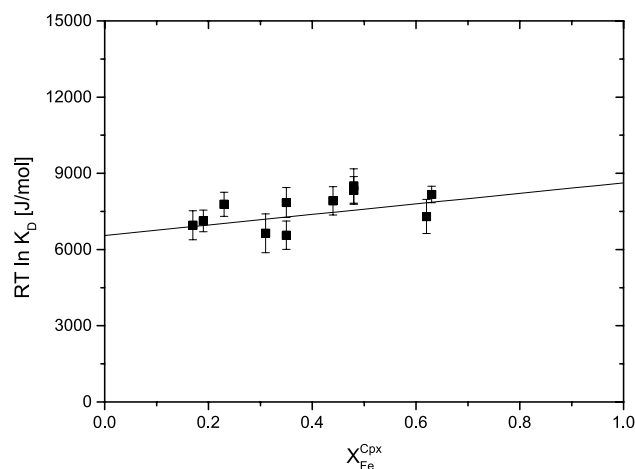


Fig. 6 $RT \ln(K_D)$, where K_D is the Fe–Mg exchange coefficient between garnet and clinopyroxene (Eq. 23), R is the gas constant and T is the temperature, versus the mole fraction of Fe in clinopyroxene. The solid line shows the fit of Eq. (24) to the experimental data in order to determine the Fe–Mg Margules interaction parameter for clinopyroxene (see text). K_D s are extracted from three multi-chamber capsule experiments containing a total of 11 individual sample chambers. The error bars indicate one standard error propagated from the microprobe analyses

to reproduce the experimental temperatures within 100 °C were excluded. Of the previous studies examined, those of Tsuno and Dasgupta (2011), Yaxley and Brey (2004), Konzett et al. (2008), and Pertermann and Hirschmann (2003) met these criteria and resulted in a refined model consistent with the experimental data from this study. Several other studies (Kiseeva et al. 2012; Spandler et al. 2008; Hammouda et al. 2009) that met the initial criteria but provided a poor fit to this model are discussed later, along with some possible explanations.

The combined data set comprises 46 experimental points between 2 and 7 GPa, and temperatures from 900 to 1,550 °C. The resulting parameters are given in Table 4 with the residuals for each experimental point, i.e., the difference in free energy across Eq. (11), plotted as a function of Al^{IV} in Fig. 7a. These residuals are in general less than 2 kJ with some values around 3 kJ. Most importantly, the residuals show no correlation with Al^{IV} or in fact any other chemical component. Expressed as ΔP between the calculated and experimental pressure as shown in Fig. 7b, the average deviation is ~ 0.2 GPa.

Discussion

Model uncertainties

The quality of the clinopyroxene chemical analyses causes the main source of uncertainty in the calculated pressure.

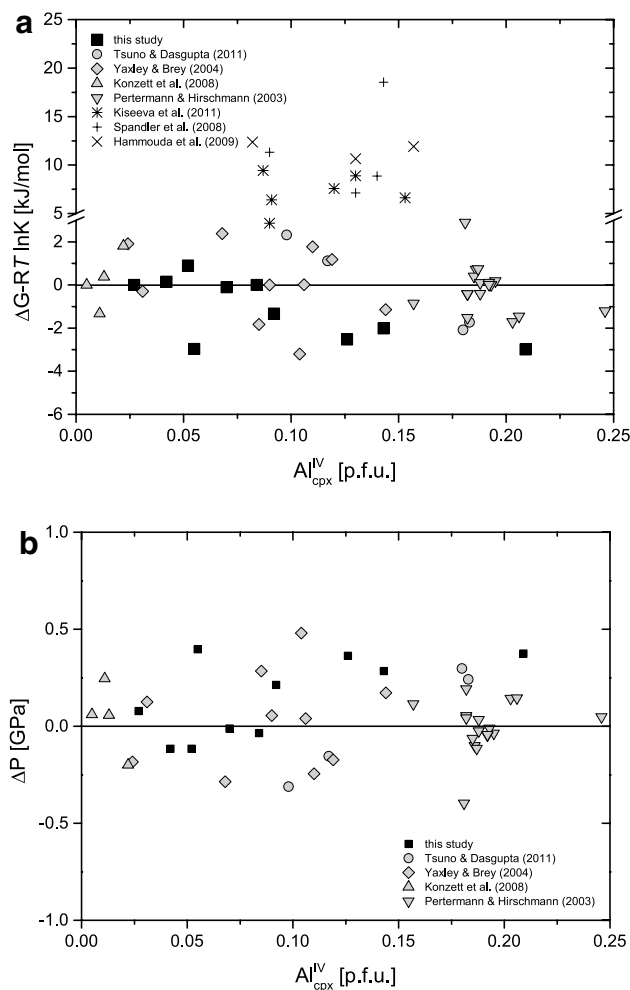


Fig. 7 **a** Residuals from the minimization of the Gibbs free energy change in Eq. (11) at the pressure and temperature of interest, plotted against the proportion of the CaTs component (i.e., cpx Al^{IV}). The experiments used in the refinement show a deviation that is generally within ± 2 kJ/mole. Several further studies show much greater residuals and were not included in the refinement. Possible reasons for this discrepancy are discussed in the text. **b** $P_{\text{calc}} - P_{\text{exp}}$ of experimental run products as a function of the CaTs component. As in **a**, no systematic variation with CaTs can be observed

The contributions to the activity term in Eq. (11) are approximately 40 % CaTs, 15 % diopside, 10 % pyrope, and 35 % grossular. Accordingly, uncertainties in the determination of the CaTs fraction have the largest impact on the calculated pressure, with uncertainties in SiO₂ analyses having by far the largest influence. When cpx Si concentrations remain below 1.985 formula units, then a 1 % uncertainty on the SiO₂ analyses propagates to a maximum uncertainty of ~ 10 % in pressure. A 5 % uncertainty on any of the other major oxides propagates to an absolute pressure uncertainty that remains below 0.1 GPa. However, once silica contents rise above 1.985 formula units, pressure uncertainties rise quickly and reach for example 25 % at ~ 1.995 formula units of Si. A Si content of around 1.985

formula units, i.e., 1.5 mol% CaTs content, is, therefore, a practical limit to the use of the barometer. This can be also expressed as a simple exponential function for the percentage error on the calculated pressure, i.e.,

$$\% \text{err} = 1.94 \times 10^{-8} e^{10.18398 * [\text{Si}]} \quad (25)$$

, where [Si] is the number of Si cations in the cpx formula. An uncertainty in the temperature of 100 °C corresponds to an uncertainty in the pressure of ~ 0.5 GPa. However, for most compositions, temperature variations will move pressure determinations along a slope that is approximately parallel to a calculated cratonic geotherm. Incorrect temperature estimates will lead to incorrect depth determinations but should not strongly influence the geotherm along which the sample lies.

The Fe³⁺ content of the mineral phases can potentially influence the determination of pressure using the barometer, primarily as it influences the determination of cation mole fractions on each site but also potentially due to non-ideal cation interactions with Fe³⁺. Because analyses of natural samples rarely include accurate Fe³⁺ determinations and only a limited number of Fe³⁺/ Σ Fe measurements were taken in the current study, all Fe is treated as Fe²⁺ in the barometer calibration and both of these influences are ignored. An estimate of at least the primary influence of Fe³⁺ on pressure determinations can be made however. Measurements (Cosca and Peacor 1987; Luth and Canil 1993) and reasoning imply that Fe³⁺ partitions preferentially onto the cpx M1 site and the octahedral (Al) site of garnet. As such, the most significant consequence for the barometer of unknown Fe³⁺/ Σ Fe ratios is on the mole fraction of Mg on the cpx M1 site and the mole fractions of Ca and Mg on the garnet dodecahedral site. Using the measurements of mineral Fe³⁺/ Σ Fe ratios measured in this study, i.e., 0.16 for garnet and 0.19 for cpx, the apparent effect on the barometer resulting from a drop in the Fe³⁺ contents of both minerals to zero, i.e., a hypothetical more reduced condition, would be an increase in the pressure by up to 0.15 GPa. As this is relatively trivial, Fe³⁺/ Σ Fe ratios of natural samples (Sobolev et al. 1999), which in most instances appear to be similar or lower than those measured in this study, can be safely assumed to be zero without major consequences. If, on the other hand, garnet that Fe³⁺/ Σ Fe ratios are higher than those determined in the experiments, then in comparison with the case where all Fe is treated as Fe²⁺, the activities of Mg and Ca in the dodecahedral site will in reality increase, but the Al activity, which is assumed to be 1 in the current study, would in effect decrease. These effects will tend to cancel out and unless strong non-ideal interactions take place, the uncertainties introduced by assuming all Fe is Fe²⁺ will be trivial. The effect on cpx is even smaller. In summary, as the experiments were performed in equilibrium with graphite

and lithospheric oxygen fugacities are typically also in the range of graphite or diamond stability (Stagno et al. 2013), the barometer can likely be applied to a wide range of mantle rocks while assuming all measured Fe is Fe^{2+} . The same argument most likely holds for diamond inclusions.

Comparison with previous studies

As described previously, the studies of Tsuno and Dasgupta (2011), Yaxley and Brey (2004), Konzett et al. (2008), and Pertermann and Hirschmann (2003) can be consistently fitted along with the current study into a refinement of the geobarometer parameters. Some data from these studies were excluded from the refinement, either because of large reported uncertainties on the chemical analyses, in particular the Al_2O_3 and SiO_2 analyses, or because the experimental temperature was not reproduced by the application of the Ellis and Green (1979) and Nakamura (2009) geothermometers by better than 100 °C. As shown in Fig. 8, the barometer reproduces the reported experimental pressures within these five studies to better than 0.2 GPa at the 1 σ level. The experimental data are only from eclogitic bulk compositions, but in addition to bimineralic assemblages, these also include silica saturated and kyanite-bearing run products (e.g., Konzett et al. 2008; Pertermann and Hirschmann 2003), for which pressures are well reproduced. The barometer has not been calibrated using samples containing orthopyroxene or olivine, however, for which other barometers are likely more suitable.

A number of further experimental studies, which were not used in the calibration, also report eclogitic mineral compositions that are consistent with the barometer (Klemme et al. 2002; Green et al. 2000; Kessel et al. 2005; Kogiso and Hirschmann 2006). Several other studies, however, that passed the tests imposed to filter out disequilibrium experiments result in significant differences when experimental and calculated pressures are compared (Kiseeva et al. 2012; Spandler et al. 2008; Hammouda et al. 2009). These differences are consistently in the same direction and arise from higher CaTs contents, generally ~0.05 formula units, in these experiments compared to those used in the refinement at similar pressures and temperatures. This leads to an underestimation in the calculated pressure compared to the experimental pressure (Fig. 8). The extent of the underestimate increases with pressure from -0.1 GPa at around 3 GPa to -2 GPa at 6 GPa. The exact cause of this discrepancy is hard to determine, though the increase in the mismatch with pressure might point at an issue in pressure calibration at high pressures. The bulk compositions employed are similar across all studies, to the extent that they mainly crystallize a bimineralic assemblage of garnet and cpx. The main variation is in the addition of volatiles, with the current study containing H_2O and

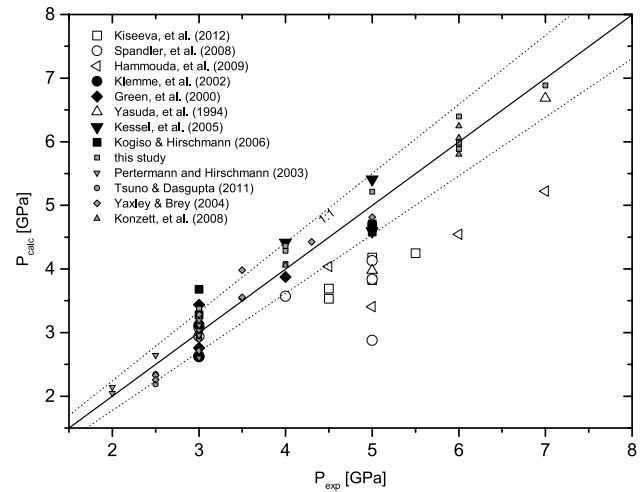


Fig. 8 Comparison between calculated and estimated pressure for a number of experimental studies conducted in eclogitic systems. Those data used in the refinement of the geobarometer are indicated by *small gray symbols*. The *dotted lines* represent the 10 % uncertainty as discussed in the text

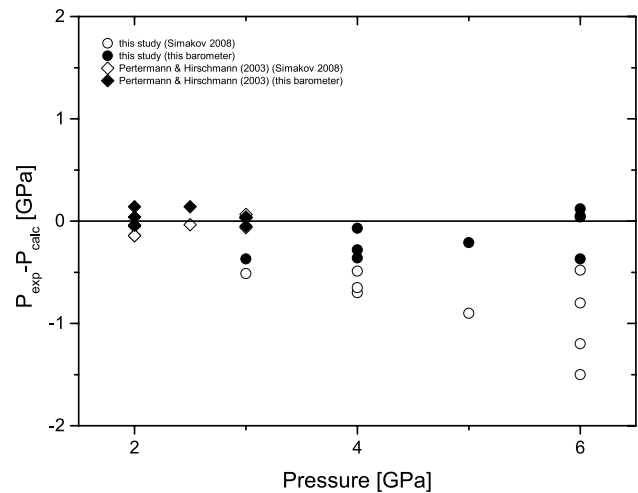


Fig. 9 Differences between experimental pressures and those calculated using the barometer refined in this study and the barometer of Simakov (2008) are shown using the experiments performed in this study and those performed at lower pressures by Pertermann and Hirschmann (2003)

F and the discrepant studies mainly performed in the presence of CO_2 . However, the studies of Tsuno and Dasgupta (2011), and Yaxley and Brey (2004) were also anhydrous and contained CO_2 and are in good agreement with this study. Another possibility would be the differences in the $\text{Fe}^{3+}/\Sigma\text{Fe}$ ratios in phases between the two groups of studies. However, there is no reason, based on the experimental procedures, to expect large differences in oxygen fugacity between the studies and, as explained in the previous

section, such differences would not be expected to have a significant effect on calculated pressures.

One explanation would be a difference in the calibrated pressure between the two groups of studies. Some indication that this is indeed an issue can be obtained by also examining the garnet majorite content, which is also a function of pressure. In this study, garnet Si contents start to rise above 3 cations per formula unit at pressures above 4 GPa and reach values of 3.05, i.e., 5 mol% majorite, by 7 GPa. This is consistent with recent thermodynamic calculations that incorporate many experimental data sets (Stixrude and Lithgow-Bertelloni 2011). The studies of Hammouda et al. (2009) and Kiseeva et al. (2012) show in general lower garnet majorite contents at comparable conditions, which would be consistent with the inferred difference in pressure between the two sets of studies based on the cpx CaTs content.

In Fig. 9, the barometer calibration is compared with a similar calibration made by Simakov (2008). Pressures for experiments performed in this study and that of Petermann and Hirschmann (2003) are calculated and compared. Both barometers are in good agreement at pressures up to 3 GPa, but at higher pressures the Simakov (2008) geobarometer predicts pressures that are systematically high compared to this study. We note that at high pressures, the experimental data set used by Simakov (2008) employs many assemblages that are not formed from eclogitic bulk compositions.

Geobarometry of mantle eclogites

The geobarometer has been used to calculate apparent equilibration pressures for a range of eclogitic mantle xenolith assemblages selected from cratonic kimberlites from various localities (Table 5). Analyses were selected for samples where clinopyroxenes contained sufficient CaTs in clinopyroxene. Furthermore, mostly pristine samples were selected that lacked significant overprinting by metamorphic events, based on the described textural observations and exsolution lamellae in clinopyroxene. The temperature for each garnet–clinopyroxene pair was determined with the Ellis and Green (1979) garnet–clinopyroxene geothermometer and cross-checked using the geothermometers of Krogh (1988) and Nakamura (2009). The pressure and temperature calculated for each assemblage is shown in Fig. 10 where the values are compared with conductive geotherms for cratonic lithosphere calculated for heat flows between 40 and 45 mWm⁻². Three sets of samples, representative of different conditions, are plotted with error bars calculated using Eq. (25). For clarity, the errors on other sample sets are not shown. Error bars reflect the uncertainties in the CaTs component, which increase with pressure and temperature as the component decreases.

Table 5 P-T calculations for various eclogite xenoliths from cratonic localities

Sample No.	T (°C) ^a	P (GPa)	Comment	Reference ^b
<i>Zero eclogite, Kuruman group, Kaapvaal craton, South Africa</i>				
Z184	1,007	3.5		1
Z323	1,044	3.3		1
Z257	852	2.2		1
Z298	809	2.3		1
Z239	720	2.2		1
<i>Kaalvallei Group II kimberlite, South Africa</i>				
295	1,201	6.2		2
384	1,121	6.0		2
385	1,041	6.4		2
394	1,152	7.8		2
413	1,141	7.0		2
415	1,160	6.1		2
<i>Mir kimberlite, Yakutia, Russia</i>				
M-432	1,070	5.3	High Ca group	3
M-69	1,100	5.1	High Ca group	3
M-54	1,050	5.1	High Ca group	3
M-60/1214	1,127	4.3	Intermediate Ca group	3
M-53/1164	829	2.5	Intermediate Ca group	3
M-53	1,002	4.4	Intermediate Ca group	3
M-2385	1,176	5.3	Low Ca group	3
M-704	1,045	4.7	Low Ca group	3
M-180	1,017	4.2	Low Ca group	3
<i>Bellsbank kimberlite, main and Bobbejaan fissure, South Africa</i>				
CK22/3	1,075	3.8		4
CK22/7	1,028	4.3		4
CK27/3	1,011	4.5		4
CK27/4	1,090	4.6		4
Ck27/7	1,011	4.0		4
<i>Roberts Victor kimberlite, South Africa</i>				
HRV247A	1,027	3.9		5
HRV247B	1,028	3.2		6
HRV247F	1,044	4.4		6
RV9A	1,138	6.0		4
RV9B	1,177	6.5		4
<i>Nunatak-1390 kimberlite, West Greenland</i>				
488585C	886	2.8	Pristine	7
592572E	894	2.9	Pristine	7
592572G	928	2.9	Pristine	7
488585B	831	3.1	Metasomatically overprinted	7
592572A	964	2.6	Metasomatically overprinted	7
592572C	905	3.1	Metasomatically overprinted	7
592572DA	955	3.2	Metasomatically overprinted	7
592572DB	987	2.8	Metasomatically overprinted	7

Table 5 continued

Sample No.	T (°C) ^a	P (GPa)	Comment	Reference ^b
<i>Eclogitic inclusions in diamonds, Namibia coast</i>				
Nam-89	1,193	5.0		8
Nam-203	1,173	5.0		8
<i>Eclogitic inclusions in diamonds, Premiere Mine, South Africa</i>				
AP101	1,301	4.6		9
AP102	1,315	5.4		9
AP106	1,358	5.4		9
AP108	1,264	5.4		9
<i>Eclogite xenoliths, Udachnaya kimberlite, Yakutia, Russia</i>				
56/2	1,138	5.0		10
112/3	1,042	4.7		10
58/2	1,273	6.3		10
55/2	1,077	4.8		10
27a/1	1,034	5.2		10
37/1	1,071	4.9		10
50/2	1,021	5.0		10
100/2	1,199	5.6		10
107/2	1,133	5.3		10

^a Temperatures calculated with the Ellis and Green (1979) thermometer, *Temperatures calculated with the Krogh (1988) geothermometer. ^bReferences: 1 Schmickler et al. (2004), 2 Viljoen et al. (2005), 3 Beard et al. (1996), 4 Carswell et al. (1981), 5 Luth et al. (1990), 6 O'Reilly and Griffin (1995), 7 Tappe et al. (2011), 8 Stachel et al. (2004), 9 Viljoen et al. (2010), 10 Jerde et al. (1993)

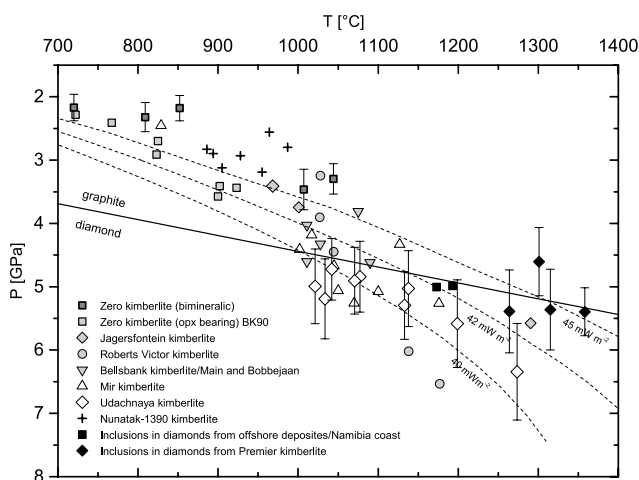


Fig. 10 Pressure–temperature calculations for natural eclogite xenoliths from several kimberlites and eclogitic diamond inclusions. The graphite–diamond transition is taken from Kennedy and Kennedy (1976). The geotherms are calculated according to Pollack and Chapman (1977). References for each sample suite are given in Table 5. Uncertainties are shown for just three representative sample sets for clarity, calculated using Eq. (25)

The lowest pressure samples investigated are from the Zero kimberlite in the Kuruman group, which come from a locality close to the edge of the Kaapvaal craton

(Schmickler et al. 2004). The biminerale eclogites indicate conditions slightly hotter than a 45 mWm^{-2} geotherm, which probably reflects their origin at the margin of the craton where the lithosphere is thinner. Orthopyroxene-bearing rocks from the same suite are also shown in Fig. 10 with pressures determined from the Al-in-orthopyroxene geobarometer of Brey et al. (1990). These also plot on or slightly above the 45 mWm^{-2} geotherm and are in reasonable agreement, particularly when errors on both barometers are considered. The biminerale- and orthopyroxene-bearing samples indicate a slightly hotter geotherm compared to that estimated from peridotitic xenoliths from the same locality (Shee et al. 1989) but this difference is again similar to the uncertainties in the pressure determinations.

A suit of eclogites from the Nunatak-1390 kimberlite boulders, West Greenland (Tappe et al. 2011), are shown in Fig. 10 revealing a relatively narrow pressure range averaging at approximately 3 GPa. The samples plot along a hotter geotherm compared to projections of the North Atlantic cratonic geotherm of Sand et al. (2009) determined from peridotite xenoliths. Based on clinopyroxene trace-element concentrations, both pristine and metasomatically overprinted assemblages can be identified within this group with the latter showing strong incompatible element enrichments (Tappe et al. 2011). Although the calculated pressures for the overprinted assemblages have a slightly larger spread than the pristine samples, average pressures determined for both suites, $2.9 \pm 0.1 \text{ GPa}$ (pristine) and $3.0 \pm 0.3 \text{ GPa}$ (overprinted), are practically identical.

Eclogitic xenoliths from the Kaapvaal craton (Jagersfontein, Roberts Victor, Bellsbank) follow geotherms between 38 and 45 mWm^{-2} , with some of the deepest eclogites in accordance with the lowest geotherm. Pressures are found to penetrate well into the diamond stability field (Roberts Victor and Jagersfontein), consistent with the diamondiferous nature of some xenoliths from these localities.

Eclogitic xenoliths from the Mir and Udachnaya kimberlites from the Siberian craton give pressures that penetrate the diamond stability field and follow a conductive mantle geotherm between 40 and 42 mWm^{-2} . This is slightly higher than that commonly assumed for the Siberian craton of around $35\text{--}40 \text{ mWm}^{-2}$ based on peridotitic samples and geophysical observations (Beard et al. 1996; Kuskov et al. 2011). These observations are, however, in reasonable agreement with those made by Ashchepkov et al. (2010) on Siberian kimberlite xenocrysts using monomineralic thermobarometry.

The geobarometer has also been used to determine the equilibration pressure of some eclogitic diamond inclusions (Shirey et al. 2013). In Fig. 10, pressures for paired inclusions are determined for diamonds from the Premier kimberlite (Viljoen et al. 2010) and for placer diamonds from the coast of Namibia (Stachel et al. 2004). The inclusions

from both locations give pressures which are within the diamond stability field. Only the inclusion AP101 from the Premier mine has calculated pressures outside of the diamond stability field when errors are included (1301 °C, 4.6 GPa).

Summary

The garnet–clinopyroxene geobarometer has been calibrated based on the pressure dependence of Ca-Tschermaks substitution in clinopyroxene. Experimental data on biminerally eclogites used in the calibration were supplemented by literature data to obtain analyses in the range of 2–7 GPa, 900–1,550 °C. The barometer can be used with limited uncertainty if mineral $\text{Fe}^{3+}/\Sigma\text{Fe}$ ratios remain below 0.2, which is consistent with values obtained in equilibrium with graphite or diamond.

The barometer calculations are inconsistent with some previous studies (Hammouda et al. 2009; Kiseeva et al. 2012; Spandler et al. 2008), although the discrepancies in pressure calculated are to some extent consistent with generally lower garnet majorite components in these studies. This may indicate that pressures have been overestimated in these previous studies. Other experimental studies in eclogitic systems which were not included in the calibration are in good agreement with the barometer and reproduce the experimental pressures within 2σ (Green et al. 2000; Kessel et al. 2005; Klemme et al. 2002; Kogiso and Hirschmann 2006). The barometer reproduces experimental pressures down to conditions of 2 GPa and 900 °C and up to approximately 7 GPa and 1,500 °C. Due to the use of a thermodynamically consistent model, these ranges can likely be extended at least in temperature down to 700 °C, although the lack of well-equilibrated experimental data at these conditions means the results should be viewed more critically. Furthermore, the phase transition in omphacite from P2/n to C2/c at approximately 865 °C at 1.5–1.8 GPa, which is not accounted for in the barometer, may also influence its use at low temperatures and pressures (Carpenter, 1982). Limits to the use of the barometer at lower temperatures and high pressures are set by the diminishing mole fraction of the Ca-Tschermaks component. The barometer should be suitable for calculating pressures of equilibration of deep crustal and upper mantle eclogite xenoliths and paired garnet–clinopyroxene diamond inclusions. Furthermore, the barometer can be applied to quartz- and kyanite-bearing eclogitic samples. Other barometers can most likely be more reliably applied to orthopyroxene-bearing assemblages.

Acknowledgments We are indebted to members of the mechanical, electronics, and polishing workshop at the BGI for their efforts in maintaining the laboratory equipment. This project was financially supported by ERC Grant no. 227893 “DEEP” funded through the EU 7th Framework Programme. We are grateful for the input from

the editor J. Blundy, S. Simakov, and one anonymous reviewer who greatly enhanced the manuscript with their contributions.

References

- Ashchepkov IV, Pokhilenko NP, Vladykin NV, Logvinova AM, Afanasiev VP, Pokhilenko LN, Kuligin SS, Malygina EV, Alymova NA, Kostrovitsky SI (2010) Structure and evolution of the lithospheric mantle beneath Siberian craton, thermobarometric study. *Tectonophysics* 485(1):17–41
- Beard B, Fraracci KN, Clayton RA, Mayeda TK, Snyder G, Sobolev N, Taylor L (1996) Petrography and geochemistry of eclogites from the Mir kimberlite, Yakutia, Russia. *Contrib Mineral Petrol* 125(4):293–310
- Boyd FR (1970) Garnet peridotites in the system $\text{CaSiO}_3\text{--MgSiO}_3\text{--Al}_2\text{O}_3$. *Mineral Soc Am Spec Pap* 3:63–75
- Brey G, Köhler T (1990) Geothermobarometry in four-phase lherzolites II. New thermobarometers, and practical assessment of existing thermobarometers. *J Petrol* 31(6):1353–1378
- Brey G, Nickel K, Kogarko L (1986) Garnet–pyroxene equilibria in the system $\text{CaO--MgO--Al}_2\text{O}_3\text{--SiO}_2$ (CMAS): prospects for simplified (‘T-independent’) lherzolite barometry and an eclogite-barometer. *Contrib Mineral Petrol* 92(4):448–455
- Brey GP, Köhler T, Nickel KG (1990) Geothermobarometry in Four-phase Lherzolites I. Experimental Results from 10 to 60 kb. *J Petrol* 31(6):1313–1352. doi:10.1093/petrology/31.6.1313
- Carpenter M (1982) Time-temperature-transformation (TTT) analysis of cation disordering in omphacite. *Contrib Mineral Petrol* 78(4):433–440. doi:10.1007/BF00375205
- Carswell D, Dawson J, Gibb F (1981) Equilibration conditions of upper-mantle eclogites: implications for kyanite-bearing and diamondiferous varieties. *Mineral Mag* 44(333):79–89
- Cartigny P (2005) Stable isotopes and the origin of diamond. *Elements* 1(2):79–84. doi:10.2113/gselements.1.2.79
- Coleman RG, Lee DE, Beatty LB, Brannock WW (1965) Eclogites and eclogites: their differences and similarities. *Geol Soc Am Bull* 76(5):483–508. doi:10.1130/0016-7606(1965)76[483:eaetda]2.0.co;2
- Cosca MA, Peacor DR (1987) Chemistry and structure of esseneite ($\text{CaFe}(\text{super } 3 +)\text{AlSiO}_6$), a new pyroxene produced by pyrometamorphism. *Am Miner* 72(1–2):148–156
- Dawson J, Carswell D (1990) High temperature and ultra-high pressure eclogites. In: Carswell DA (ed) *Eclogite facies rocks*. Blackie, Glasgow London, pp 314–349
- Ellis DJ, Green DH (1979) An experimental study of the effect of Ca upon garnet–clinopyroxene Fe–Mg exchange equilibria. *Contrib Mineral Petrol* 71(1):13–22. doi:10.1007/bf00371878
- Ganguly J, Cheng WJ, Tirone M (1996) Thermodynamics of aluminosilicate garnet solid solution: new experimental data, an optimized model, and thermometric applications. *Contrib Mineral Petrol* 126(1–2):137–151. doi:10.1007/s004100050240
- Gasparik T (1996) Diopside–jadeite join at 16–22 GPa. *Phys Chem Miner* 23(7):476–486. doi:10.1007/BF00202034
- Green TH, Blundy JD, Adam J, Yaxley GM (2000) SIMS determination of trace element partition coefficients between garnet, clinopyroxene and hydrous basaltic liquids at 2–7.5 GPa and 1080–1200°C. *Lithos* 53(3–4):165–187. doi:10.1016/S0024-4937(00)00023-2
- Griffin WL, O’Reilly SY, Abe N, Aulbach S, Davies RM, Pearson NJ, Doyle BJ, Kivi K (2003) The origin and evolution of Archean lithospheric mantle. *Precambr Res* 127(1–3):19–41. doi:10.1016/S0301-9268(03)00180-3
- Hammouda T, Moine B, Devidal J-L, Vincent C (2009) Trace element partitioning during partial melting of carbonated eclogites. *Phys Earth Planet Inter* 174(1):60–69

- Helmstaedt H, Doig R (1975) Eclogite nodules from kimberlite pipes of the Colorado Plateau—samples of subducted Franciscan-type oceanic lithosphere. *Phys Chem Earth* 9:95–111
- Herzberg CT (1978) Pyroxene geothermometry and geobarometry: experimental and thermodynamic evaluation of some subsolidus phase relations involving pyroxenes in the system CaO–MgO–Al₂O₃–SiO₂. *Geochim Cosmochim Acta* 42(7):945–957
- Holland T, Powell R (2011) An improved and extended internally consistent thermodynamic dataset for phases of petrological interest, involving a new equation of state for solids. *J Metamorph Geol* 29(3):333–383
- Jacob DE (2004) Nature and origin of eclogite xenoliths from kimberlites. *Lithos* 77(1–4):295–316. doi:10.1016/j.lithos.2004.03.038
- Jerde EA, Taylor LA, Crozaz G, Sobolev NV, Sobolev VN (1993) Diamondiferous eclogites from Yakutia, Siberia: evidence for a diversity of protoliths. *Contrib Mineral Petrol* 114(2):189–202
- Kennedy CS, Kennedy GC (1976) The equilibrium boundary between graphite and diamond. *J Geophys Res* 81(14):2467–2470
- Keppeler H, Frost DJ (2005) Introduction to minerals under extreme conditions. *Mineral Behav Extreme Cond EMU Notes Mineral* 7:1–30
- Kessel R, Ulmer P, Pettko T, Schmidt M, Thompson A (2005) The water–basalt system at 4 to 6 GPa: phase relations and second critical endpoint in a K-free eclogite at 700 to 1400 °C. *Earth Planet Sci Lett* 237(3):873–892
- Kiseeva ES, Yaxley GM, Hermann J, Litasov KD, Rosenthal A, Kamenetsky VS (2012) An experimental study of carbonated eclogite at 3–5–5 GPa—implications for silicate and carbonate metasomatism in the cratonic mantle. *J Petrol* 53(4):727–759
- Klemme S, Blundy JD, Wood BJ (2002) Experimental constraints on major and trace element partitioning during partial melting of eclogite. *Geochim Cosmochim Acta* 66(17):3109–3123. doi:10.1016/s0016-7037(02)00859-1
- Kogiso T, Hirschmann MM (2006) Partial melting experiments of biminerally eclogite and the role of recycled mafic oceanic crust in the genesis of ocean island basalts. *Earth Planet Sci Lett* 249(3–4):188–199. doi:10.1016/j.epsl.2006.07.016
- Konzett J, Frost DJ, Proyer A, Ulmer P (2008) The Ca–Eskola component in eclogitic clinopyroxene as a function of pressure, temperature and bulk composition: an experimental study to 15 GPa with possible implications for the formation of oriented SiO₂-inclusions in omphacite. *Contrib Mineral Petrol* 155(2):215–228
- Koons PO (1984) Implications to garnet–clinopyroxene geothermometry of non-ideal solid solution in jadeitic pyroxenes. *Contrib Mineral Petrol* 88(4):340–347
- Krogh EJ (1988) The garnet–clinopyroxene Fe–Mg geothermometer—a reinterpretation of existing experimental data. *Contrib Mineral Petrol* 99(1):44–48
- Kuskov OL, Kronrod VA, Prokof'ev AA (2011) Thermal structure and thickness of the lithospheric mantle underlying the Siberian Craton from the kraton and kimberlit superlong seismic profiles. *Izv Phys Solid Earth* 47(3):155–175. doi:10.1134/s1069351310111011
- Lehnert K, Su Y, Langmuir CH, Sarbas B, Nohl U (2000) A global geochemical database structure for rocks. *Geochem Geophys Geosyst* 1(5):1–14. doi:10.1029/1999gc000026
- Liou JG, Ernst WG, Zhang RY, Tsujimori T, Jahn BM (2009) Ultra-high-pressure minerals and metamorphic terranes—the view from China. *J Asian Earth Sci* 35(3–4):199–231. doi:10.1016/j.jseaes.2008.10.012
- Liu Y, Taylor LA, Sarbadhikari AB, Valley JW, Ushikubo T, Spicuzza MJ, Kita N, Ketcham RA, Carlson W, Shatsky V (2009) Metasomatic origin of diamonds in the world's largest diamondiferous eclogite. *Lithos* 112:1014–1024
- Luth R, Canil D (1993) Ferric iron in mantle-derived pyroxenes and a new oxybarometer for the mantle. *Contrib Mineral Petrol* 113(2):236–248. doi:10.1007/bf00283231
- Luth R, Virgo D, Boyd F, Wood B (1990) Ferric iron in mantle-derived garnets. *Contrib Mineral Petrol* 104(1):56–72. doi:10.1007/bf00310646
- MacGregor ID, Manton WI (1986) Roberts victor eclogites: ancient oceanic crust. *J Geophys Res Solid Earth* 91(B14):14063–14079. doi:10.1029/JB091iB14p14063
- Mukhopadhyay B (1991) Garnet–clinopyroxene geobarometry—the problems, a prospect, and an approximate solution with some applications. *Am Miner* 76(3–4):512–529
- Nakamura D (2009) A new formulation of garnet–clinopyroxene geothermometer based on accumulation and statistical analysis of a large experimental data set. *J Metamorph Geol* 27(7):495–508. doi:10.1111/j.1525-1314.2009.00828.x
- Newton R (1986) Metamorphic temperatures and pressures of Group B and C eclogites. *Geol Soc Am Mem* 164:17–30
- Newton R, Perkins D (1982) Thermodynamic calibration of geobarometers based on the assemblages garnet–plagioclase–orthopyroxene (clinopyroxene)–quartz. *Am Miner* 67(3–4):203–222
- Nickel K, Green D (1985) Empirical geothermobarometry for garnet peridotites and implications for the nature of the lithosphere, kimberlites and diamonds. *Earth Planet Sci Lett* 73(1):158–170
- Nikitina L (2000) Garnet–orthopyroxene and garnet–clinopyroxene thermobarometers for mantle xenoliths. *Capricious earth: models and modelling of geologic processes and objects*. Eds Glebovitsky VA, Dech VN Theophrastus *Contrib Adv Stud Geol* 3:44–53
- Nimis P, Taylor WR (2000) Single clinopyroxene thermobarometry for garnet peridotites. Part I. Calibration and testing of a Cr–Cpx barometer and an enstatite–in–Cpx thermometer. *Contrib Mineral Petrol* 139(5):541–554. doi:10.1007/s004100000156
- Nimis P, Ulmer P (1998) Clinopyroxene geobarometry of magmatic rocks Part I: an expanded structural geobarometer for anhydrous and hydrous, basic and ultrabasic systems. *Contrib Mineral Petrol* 133(1–2):122–135. doi:10.1007/s004100050442
- Ono S, Yasuda A (1996) Compositional change of majoritic garnet in a MORB composition from 7 to 17 GPa and 1400 to 1600 degrees C. *Phys Earth Planet Inter* 96(2–3):171–179. doi:10.1016/0031-9201(96)03149-4
- O'Reilly SY, Griffin W (1995) Trace-element partitioning between garnet and clinopyroxene in mantle-derived pyroxenites and eclogites: P–T–X controls. *Chem Geol* 121(1):105–130
- Pertermann M, Hirschmann MM (2003) Anhydrous partial melting experiments on MORB-like eclogite: phase relations, phase compositions and mineral–melt partitioning of major elements at 2–3 GPa. *J Petrol* 44(12):2173–2201. doi:10.1093/petrology/egg074
- Pollack HN, Chapman DS (1977) On the regional variation of heat flow, geotherms, and lithospheric thickness. *Tectonophysics* 38(3):279–296
- Purwin H, Lauterbach S, Brey GP, Woodland AB, Kleebe H-J (2013) An experimental study of the Fe oxidation states in garnet and clinopyroxene as a function of temperature in the system CaO–FeO–Fe₂O₃–MgO–Al₂O₃–SiO₂: implications for garnet–clinopyroxene geothermometry. *Contrib Mineral Petrol* 1–17
- Rapp RP, Watson EB, Miller CF (1991) Partial melting of amphibolite/eclogite and the origin of Archean trondhjemites and tonalites. *Precambrian Res* 51(1–4):1–25. doi:10.1016/0301-9268(91)90092-0
- Sand KK, Waight TE, Pearson DG, Nielsen TF, Makovicky E, Hutchison MT (2009) The lithospheric mantle below southern West Greenland: a geothermobarometric approach to diamond potential and mantle stratigraphy. *Lithos* 112:1155–1166
- Schmickler B, Jacob D, Foley S (2004) Eclogite xenoliths from the Kuruman kimberlites, South Africa: geochemical fingerprinting of deep subduction and cumulate processes. *Lithos* 75(1):173–207
- Schulze DJ (1989) Constraints on the abundance of eclogite in the upper mantle. *J Geophys Res Solid Earth* 94(B4):4205–4212. doi:10.1029/JB094iB04p04205

- Shee S, Bristow J, Bell D, Smith C, Allsopp H, Shee P (1989) The petrology of kimberlites, related rocks and associated mantle xenoliths from the Kuruman Province, South Africa. *Geol Soc Aust Spec Publ* 14:60–81
- Shirey SB, Carlson RW, Richardson SH, Menzies A, Gurney JJ, Pearson DG, Harris JW, Wiechert U (2001) Archean emplacement of eclogitic components into the lithospheric mantle during formation of the Kaapvaal Craton. *Geophys Res Lett* 28(13):2509–2512. doi:10.1029/2000GL012589
- Shirey SB, Cartigny P, Frost DJ, Keshav S, Nestola F, Nimis P, Pearson DG, Sobolev NV, Walter MJ (2013) Diamonds and the geology of mantle carbon. *Rev Mineral Geochem* 75(1):355–421
- Simakov SK (2008) Garnet–clinopyroxene and clinopyroxene geothermobarometry of deep mantle and crust eclogites and peridotites. *Lithos* 106(1–2):125–136. doi:10.1016/j.lithos.2008.06.013
- Simakov SK, Taylor LA (2000) Geobarometry for mantle eclogites: solubility of Ca-Tschermaks in clinopyroxene. *Int Geol Rev* 42(6):534–544
- Smart KA, Heaman LM, Chacko T, Simonetti A, Kopylova M, Mah D, Daniels D (2009) The origin of high-MgO diamond eclogites from the Jericho Kimberlite, Canada. *Earth Planet Sci Lett* 284(3):527–537
- Smyth JR, Caporuscio FA, McCormick TC (1989) Mantle eclogites: evidence of igneous fractionation in the mantle. *Earth Planet Sci Lett* 93(1):133–141
- Sobolev VN, McCammon CA, Taylor LA, Snyder GA, Sobolev NV (1999) Precise Mossbauer milliprobe determination of ferric iron in rock-forming minerals and limitations of electron microprobe analysis. *Am Miner* 84:78–85
- Spandler C, Yaxley G, Green DH, Rosenthal A (2008) Phase relations and melting of anhydrous K-bearing eclogite from 1200 to 1600 C and 3 to 5 GPa. *J Petrol* 49(4):771–795
- Stachel T, Harris JW (2008) The origin of cratonic diamonds—constraints from mineral inclusions. *Ore Geol Rev* 34(1–2):5–32. doi:10.1016/j.oregeorev.2007.05.002
- Stachel T, Aulbach S, Brey GP, Harris JW, Leost I, Tappert R, Viljoen KS (2004) The trace element composition of silicate inclusions in diamonds: a review. *Lithos* 77(1–4):1–19. doi:10.1016/j.lithos.2004.03.027
- Stagno V, Ojwang DO, McCammon CA, Frost DJ (2013) The oxidation state of the mantle and the extraction of carbon from Earth's interior. *Nature* 493(7430):84–88
- Stixrude L, Lithgow-Bertelloni C (2011) Thermodynamics of mantle minerals—II. Phase equilibria. *Geophys J Int* 184(3):1180–1213. doi:10.1111/j.1365-246X.2010.04890.x
- Tappe S, Smart KA, Pearson DG, Steenfelt A, Simonetti A (2011) Craton formation in Late Archean subduction zones revealed by first Greenland eclogites. *Geology* 39(12):1103–1106
- Taylor LA, Neal CR (1989) Eclogites with oceanic crustal and mantle signatures from the Bellsbank kimberlite, South Africa, Part I: mineralogy, petrography, and whole rock chemistry. *J Geol* 97(5):551–567. doi:10.2307/30078363
- Tsuno K, Dasgupta R (2011) Melting phase relation of nominally anhydrous, carbonated pelitic-eclogite at 2.5–3.0 GPa and deep cycling of sedimentary carbon. *Contrib Mineral Petrol* 161(5):743–763
- van Aken PA, Liebscher B (2002) Quantification of ferrous/ferric ratios in minerals: new evaluation schemes of Fe L 2,3 electron energy-loss near-edge spectra. *Phys Chem Miner* 29(3):188–200. doi:10.1007/s00269-001-0222-6
- van Aken PA, Liebscher B, Styrsa VJ (1998) Quantitative determination of iron oxidation states in minerals using Fe L 2,3 -edge electron energy-loss near-edge structure spectroscopy. *Phys Chem Miner* 25(5):323–327. doi:10.1007/s002690050122
- Viljoen K, Schulze D, Quadling A (2005) Contrasting group I and Group II eclogite xenolith petrogenesis: petrological, trace element and isotopic evidence from eclogite, garnet-websterite and alkremite xenoliths in the Kaalvallei kimberlite, South Africa. *J Petrol* 46(10):2059–2090
- Viljoen F, Dobbe R, Harris J, Smit B (2010) Trace element chemistry of mineral inclusions in eclogitic diamonds from the Premier (Cullinan) and Finsch kimberlites, South Africa: implications for the evolution of their mantle source. *Lithos* 118(1):156–168
- Walter MJ (1998) Melting of garnet peridotite and the origin of komatiite and depleted lithosphere. *J Petrol* 39(1):29–60. doi:10.1093/ptro/39.1.29
- Wood BJ, Banno S (1973) Garnet-orthopyroxene and orthopyroxene-clinopyroxene relationships in simple and complex systems. *Contrib Mineral Petrol* 42(2):109–124
- Wood BJ, Nicholls J (1978) The thermodynamic properties of reciprocal solid solutions. *Contrib Mineral Petrol* 66(4):389–400
- Woodland AB, O'Neill HS (1997) Thermodynamic data for Fe-bearing phases obtained using noble metal alloys as redox sensors. *Geochim Cosmochim Acta* 61(20):4359–4366. doi:10.1016/s0016-7037(97)00247-0
- Yaxley GM, Brey GP (2004) Phase relations of carbonate-bearing eclogite assemblages from 2.5 to 5.5 GPa: implications for petrogenesis of carbonatites. *Contrib Mineral Petrol* 146(5):606–619
- Zhao S, Nee P, Green HW, Dobrzhinetskaya LF (2011) Ca-Eskola component in clinopyroxene: experimental studies at high pressures and high temperatures in multianvil apparatus. *Earth Planet Sci Letters* 307(3–4):517–524. doi:10.1016/j.epsl.2011.05.026